U.S. Department of Transportation

Federal Railroad Administration

Thermodynamic and Dynamic Assessment of Solid Oxide Fuel Cell Hybrid Systems for Use in Locomotives

Office of Research,
Development
and Technology
Washington, DC 20590

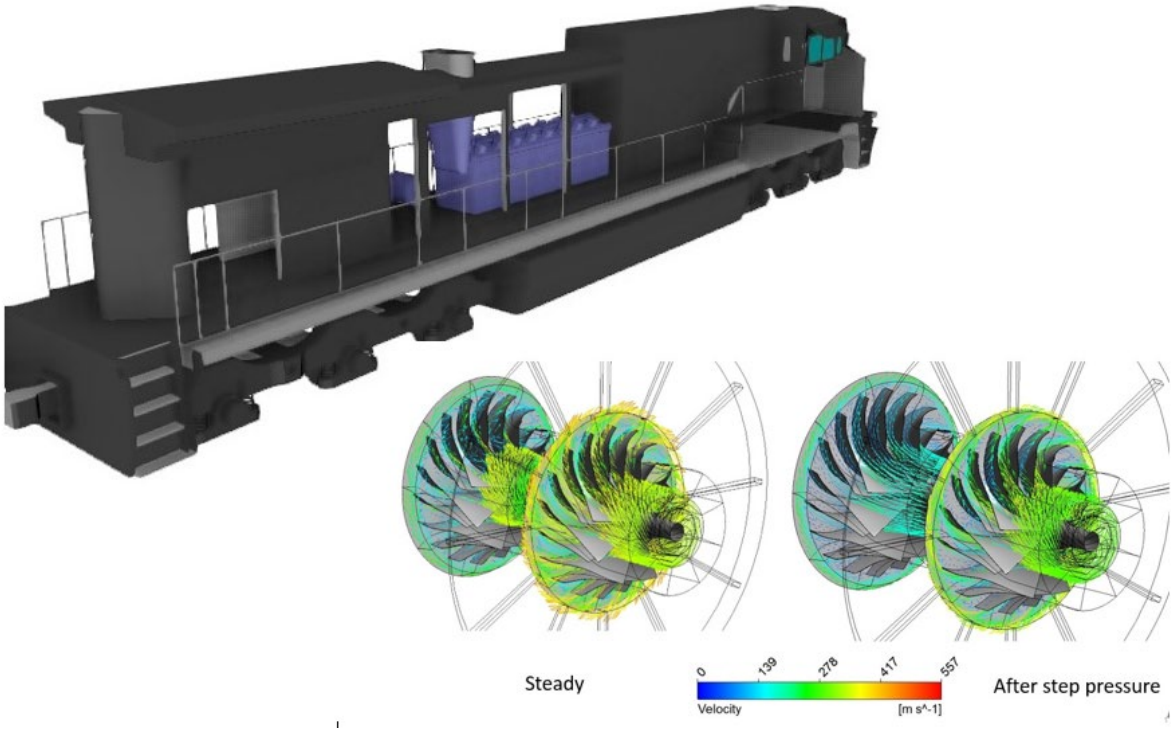

DOT/FRA/ORD-19/16

Final Report
June 2019

REPORT DOCUMENTATION PAGE

Form Approved
OMB No. 0704-0188

1. AGENCY USE ONLY (Leave blank)	2. REPORT DATE	3. REPORT TYPE AND DATES COVERED
	June 2019	Technical Report Aug. 2015-Dec. 2017

4. TITLE AND SUBTITLE
Thermodynamic and Dynamic Assessment of Solid Oxide Fuel Cell Hybrid Systems for Use in Locomotives

5. FUNDING NUMBERS
DTFR53-15-C-00024

6. AUTHOR(S)
Jacob Brouwer and Ali Azizi

7. PERFORMING ORGANIZATION NAME(S) AND ADDRESS(ES)
National Fuel Cell Research Center
University of California, Irvine
Irvine, CA 92697

8. PERFORMING ORGANIZATION REPORT NUMBER

9. SPONSORING/MONITORING AGENCY NAME(S) AND ADDRESS(ES)
U.S. Department of Transportation
Federal Railroad Administration
Office of Railroad Policy and Development
Office of Research, Development and Technology
Washington, DC 20590

10. SPONSORING/MONITORING AGENCY REPORT NUMBER
DOT/FRA/ORD-19/16

11. SUPPLEMENTARY NOTES
COR: Melissa Shurland

12a. DISTRIBUTION/AVAILABILITY STATEMENT
This document is available to the public through the FRA website.

12b. DISTRIBUTION CODE

13. ABSTRACT (Maximum 200 words)
The purpose of this investigation was to validate the feasible use of one of the currently available industrial gas turbine engines (i.e., the 200 kW C-200 engine of Capstone Turbines) in the hybrid fuel cell gas turbine test system for locomotive application. The National Fuel Cell Research Center (NFCRC) developed a full 500 kW dynamic computer model of hybrid fuel cell gas turbine system components for a test locomotive engine and demonstrated that the Capstone C-200 micro gas turbine integrated into a 500 kW hybrid solid oxide fuel cell-gas turbine (SOFC-GT) system is a viable possible option for locomotive applications. In addition, a new MATLAB code was developed and applied to integrating the gas turbine with both a Bloom Energy 200 kW SOFC system and a Versa Power 400 kW SOFC system.

14. SUBJECT TERMS
Hybrid solid oxide fuel cell-gas turbine system, SOFC-GT, National Fuel Cell Research Center, NFCRC, gas turbine, GT, locomotive, hybrid fuel cell gas turbine test system

15. NUMBER OF PAGES
69

16. PRICE CODE

17. SECURITY CLASSIFICATION OF REPORT	18. SECURITY CLASSIFICATION OF THIS PAGE	19. SECURITY CLASSIFICATION OF ABSTRACT	20. LIMITATION OF ABSTRACT
Unclassified	Unclassified	Unclassified	

METRIC/ENGLISH CONVERSION FACTORS

ENGLISH TO METRIC	METRIC TO ENGLISH
LENGTH (APPROXIMATE)	**LENGTH (APPROXIMATE)**
1 inch (in) = 2.5 centimeters (cm)	1 millimeter (mm) = 0.04 inch (in)
1 foot (ft) = 30 centimeters (cm)	1 centimeter (cm) = 0.4 inch (in)
1 yard (yd) = 0.9 meter (m)	1 meter (m) = 3.3 feet (ft)
1 mile (mi) = 1.6 kilometers (km)	1 meter (m) = 1.1 yards (yd)
	1 kilometer (km) = 0.6 mile (mi)
AREA (APPROXIMATE)	**AREA (APPROXIMATE)**
1 square inch (sq in, in^2) = 6.5 square centimeters (cm^2)	1 square centimeter (cm^2) = 0.16 square inch (sq in, in^2)
1 square foot (sq ft, ft^2) = 0.09 square meter (m^2)	1 square meter (m^2) = 1.2 square yards (sq yd, yd^2)
1 square yard (sq yd, yd^2) = 0.8 square meter (m^2)	1 square kilometer (km^2) = 0.4 square mile (sq mi, mi^2)
1 square mile (sq mi, mi^2) = 2.6 square kilometers (km^2)	10,000 square meters (m^2) = 1 hectare (ha) = 2.5 acres
1 acre = 0.4 hectare (he) = 4,000 square meters (m^2)	
MASS - WEIGHT (APPROXIMATE)	**MASS - WEIGHT (APPROXIMATE)**
1 ounce (oz) = 28 grams (gm)	1 gram (gm) = 0.036 ounce (oz)
1 pound (lb) = 0.45 kilogram (kg)	1 kilogram (kg) = 2.2 pounds (lb)
1 short ton = 2,000 pounds(lb) = 0.9 tonne (t)	1 tonne (t) = 1,000 kilograms (kg) = 1.1 short tons
VOLUME (APPROXIMATE)	**VOLUME (APPROXIMATE)**
1 teaspoon (tsp) = 5 milliliters (ml)	1 milliliter (ml) = 0.03 fluid ounce (fl oz)
1 tablespoon (tbsp) = 15 milliliters (ml)	1 liter (l) = 2.1 pints (pt)
1 fluid ounce (fl oz) = 30 milliliters (ml)	1 liter (l) = 1.06 quarts (qt)
1 cup (c) = 0.24 liter (l)	1 liter (l) = 0.26 gallon (gal)
1 pint (pt) = 0.47 liter (l)	
1 quart (qt) = 0.96 liter (l)	
1 gallon (gal) = 3.8 liters (l)	
1 cubic foot (cu ft, ft^3) = 0.03 cubic meter (m^3)	1 cubic meter (m^3) = 36 cubic feet (cu ft, ft^3)
1 cubic yard (cu yd, yd^3) = 0.76 cubic meter (m^3)	1 cubic meter (m^3) = 1.3 cubic yards (cu yd, yd^3)
TEMPERATURE (EXACT)	**TEMPERATURE (EXACT)**
[(x-32)(5/9)] °F = y °C	[(9/5) y + 32] °C = x °F

QUICK INCH - CENTIMETER LENGTH CONVERSION

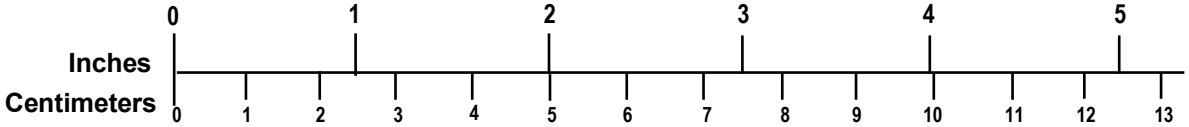

QUICK FAHRENHEIT - CELSIUS TEMPERATURE CONVERSIO

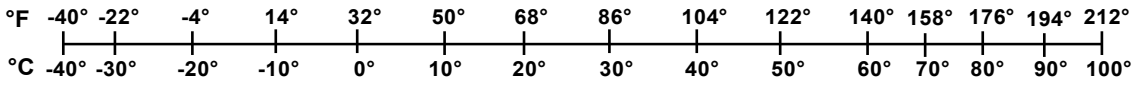

For more exact and or other conversion factors, see NIST Miscellaneous Publication 286, Units of Weights and Measures. Price $2.50 SD Catalog No. C13 10286

Updated 6/17/98

Contents

Illustrations

Tables

Executive Summary

The purpose of this investigation was to validate the feasible use of one of the currently available industrial gas turbine engines (i.e., the 200 kW C-200 system from Capstone Turbines) in a hybrid fuel cell gas turbine (FC-GT) test system for locomotive application. The Federal Railroad Administration funded the National Fuel Cell Research Center (NFCRC) at the University of California, Irvine (UCI) to develop a full 500 kW dynamic computer model of hybrid FC-GT system components for a test locomotive engine and to demonstrate that the C-200 Capstone micro gas turbine integrated into a 500-kW hybrid solid oxide fuel cell-gas turbine (SOFC-GT) system is a viable option for locomotive applications. This research was conducted between August 20, 2015, and December 31, 2017. In addition, a new MATLAB code was developed and applied to the Bloom Energy 200 kW solid oxide fuel cell (SOFC) system and Versa Power 400 kW. Using the computational fluid dynamics (CFD) model, the single-stage 200 kW C-200 gas turbine compressor is modeled in the ANSYS software platform. The pressurized air remaining in the hybrid system plenum is used as a boundary condition to solve the transient turbomachinery problem.

The possibility of industrial compressor usage in the hybrid SOFC-GT system relies on the capability of maintaining sustained flow rate throughout the compressor. The shear stress transport (SST) fluid dynamics model at high Reynolds number is used as a method of choice for the CFD problem to capture the shear stress generated by the impeller surface on the fluid domain. Control algorithms previously developed at NFCRC are used to keep the compressor flow in a safe region of operation. CFD calculations serve the purpose of validating previously developed control methods for safe operation of radial compressors, and allowing analysis of specific types of industrial compressors for this specific hybrid locomotive.

To investigate the surge/stall phenomena in C-200 micro gas turbine, two steps of power demand change were considered in the CFD analysis. Step power demand that has a similar profile to the locomotive engine power demand has been applied to the C-200 kW gas turbine as integrated with both a Bloom Energy and a Versa Power (now FuelCell Energy) solid oxide fuel cell system. The step power demand from base load to full load of 268 kW for the Bloom Energy SOFC is applied to the dynamic model. Since only 100 kW power is required out of the C-200 gas turbine for this NFCRC design, the step power demand from base load to 100 kW full load is applied to the CFD model of a gas turbine (GT) and the MATLAB code. As the power demand rises from steady state base load to full load in a short time period, the turbine inlet temperature (TIT) increases so that the GT could meet the power demand. Thus, the mass flow rate decreases due to the lower density of hot gas at the turbine inlet. However, the mass flow from the compressor persists causing a pressure buildup at the turbine inlet, increasing the local pressure. As a result of this pressure build up in the compressor outlet, a complete reversal of flow in the impellers can occur, which is called deep surge, and/or an oscillatory flow rate could occur in the impellers that is called mild surge. Figure 1 found in Section 1.1.1 shows the mechanism of stall/surge in a compressor due to the increase in TIT [17].

The results of the CFD analysis, shows that the flow in the 1.7MW Kawasaki compressor possess mild surge characteristics in the first 25 rotor revolutions. However, after 25 shaft revolutions, the compressor returns to normal operation with a sustained air mass flow rate throughout the impellers.

The previous MATLAB/Simulink dynamic model developed at NFCRC is used to size the full-scale 4 MW hybrid SOFC-GT engine for a long-haul locomotive. Sizing of the heat exchangers, fuel cell system, balance of power (BOP), piping, insulation and steam/diesel reformer were part of the

modeling effort. The mass flow rate throughout the system components is used to size the system heat exchangers (fuel preheater and recuperator heat exchangers in hybrid SOFC-GT system). The heat generated in the SOFC and catalytic combustor is used to size the insulation required for the system. The fin and plate heat exchanger uses ASPEN simulation software in conjunction with CFD simulation for validation. The fin and plate heat exchangers are chosen over shell and tube heat exchangers due to the compactness, however, manufacturing cost of the heat exchangers has not been included in the analyses yet. The schematic of the 500 kW prototype test system is under development. This 500 kW system consists of a SOFC manufactured by one of the main SOFC producing companies (i.e., Versa Power) and a 200 kW micro GT (i.e., from Capstone Turbines).

For locomotive applications, a larger gas turbine engine will be required, such as the 1.7 MW Kawasaki gas turbine was used in the model for evaluating the hybrid SOFC-GT engine in a GE dash 9 locomotive application. The dynamic model represents a platform for the locomotive engine. Due to the inability of the dynamic model to capture the nodal pressure accumulation throughout the system, especially between the compressor outlet and turbine inlet, the CFD model had to be developed to simulate the high-risk point of the thermodynamic cycle. This risk is associated with compressor failure, and complete hybrid system failure. To fully commercialize the hybrid FC-GT system, these challenges should be specifically addressed using computational tools.

1. Introduction

FRA funded research between August 20, 2015, and December 31, 2017, to investigate the feasibility of SOFC-GT as an alternative power source for locomotives. The research was performed by NFCRC at the University of California, Irvine. NFCRC developed a full 500 kW dynamic computer model of hybrid FC-GT system components for a test locomotive engine and demonstrated that the C-200 Capstone micro gas turbine integrated into a 500-kW hybrid solid oxide fuel cell-gas turbine (SOFC-GT) system is a viable option for locomotive applications. Siemens-Westinghouse Power Corporation developed the first pressurized (3 atm) hybrid SOFC-GT system that generated 220 kW of electrical power at a net electrical efficiency of 55 percent. Reduction in fossil energy resources have urged the GT industry to consider more energy efficient strategies with reduced emissions for stationary power plants. These strategies include GTs, steam turbines and reciprocating engines power plants [20]. Integrated hybrid systems have the potential to operate at a higher efficiency than a fuel cell or GT. Solid oxide fuel cells (SOFC) are the electrochemical devices that convert the chemical energy contained in fuel directly to electrical energy through electrochemical reaction. The SOFC power plant was proven as an alternative power generation technology in electric utility and for domestic, industrial and commercial applications. These types of power generation plants were presented in both locomotive and stationary applications [1] [3] [6] [12] [13] [22] [24]. SOFC has operated on various types of fuels such as carbon monoxide, natural gas, hydrogen (H_2), propane (C_3H_8), landfill gas, diesel and jet propellant, JP-8 [2] [11] [18] [25].

Typically, the operating temperature of SOFC is higher than the other types of fuel cells such as proton exchange membrane fuel cell, alkaline fuel cell, and molten carbonate fuel cell [19] [20]. Higher operating temperatures of SOFC enables them to directly reform natural gas. SOFC converts the reformed hydrogen through an electrochemical reaction and produces electrical power as well as high grade waste heat for a combined heat and power system. SOFC power generation systems operate in the power production range of 250 kW to 20 MW. Hybrid FC-GT systems provide clean energy at high efficiency [28]. The only conventional device that has been previously tested for hybrid fuel cell systems is micro-gas turbine generator (MTG). MTG has been shown amenable to integration with a high temperature SOFC. FC-GT hybrid power systems provide the highest efficiency and the cleanest emissions of all fossil fueled power plants [27]. Today, SOFC-GT hybrid systems are known as one of the most promising technologies that could meet the U.S. Department of Energy (DOE) demands [21]: 1) To achieve a higher energy efficiency, 2) minimization of environmental pollution, 3) electricity production at a competitive cost, and 4) investigation of CO_2 capture and sequestration strategies.

Some of the FC-GT challenges mentioned by Brouwer et al. are tabulated in Table 1 [2].

Table 1. SOFC-GT Hybrid System Challenges [2].

SOFC-GT hybrid system challenges
Compressor surge
High capital cost of fuel cell
Transient control
Designing a proper heat engine that could be integrated with fuel cell
GT pressure ratio and mass flow do not match the SOFC

The current study aims to provide a compressor stall/surge insight into a similar power rated hybrid SOFC-GT system.

1.1 Background

Air quality concerns and climate change due to increasing greenhouse gas emissions from combustion together with unsustainable conversion of fossil energy resources have urged the power generation community to consider more energy efficient strategies with reduced emissions for stationary power plants. Various advanced technologies have emerged including advanced aero-derivative GT systems, advanced steam turbines and combined gas/steam cycle power plants, as well as the relatively smaller, still highly efficient, and low emissions reciprocating engine power plants. Fuel cell technology has emerged as one of the most promising high efficiency and low emissions technologies for distributed generations.

Among the features that allow the integration of GT with SOFC, the following points could be made: 1) SOFC exhaust temperature and GT inlet temperature are well-matched, 2) GTs operate at relatively lower pressure ratios that makes integration easier, 3) GTs often use recuperation in order to improve the system efficiency, 4) GTs allow fuel cells to operate under higher pressures which improves the cell performance, and 5) thermal energy amount and quality (temperature) contained in the SOFC exhaust is sufficient for GT inlet conditions to produce compressor power (for the fuel cell pressurization) and an electric power generator (that produces additional electricity) [2].

Some of the hybrid FC-GT challenges previously identified by Brouwer et al. are listed in Table 1 [2]. However, compressor surge is the focus of the current investigation. All FC-GT systems are characterized by a relatively large volume of gas between the air compressor and the turbine, due to the presence of a large volume fuel cell in place of a small volume combustor in the hybrid cycle. This large volume allows for the storage of GT working fluid and increased pressure dynamics during hybrid system dynamic operation. These increased pressure fluctuations can lead to conditions of compressor surge/stall.

1.1.1 Introduction to Surge in Hybrid Fuel Cell-Gas Turbine System

Placing the fuel cell in a high pressure section between the compressor and turbine increases the fuel cell efficiency by increasing reactant and product partial pressures and lowering polarization effects. This topping cycle design introduces the need for a pressure vessel and increases the potential for compressor stall/surge as outlined above. Under steady-state conditions the compressor supplies a specific mass flow rate of air at every combination of shaft speed and pressure ratio. These values are typically normalized and compiled into tables or plotted in compressor maps. At specific pressure

ratios and shaft speeds, compressor surge occurs when a reversal of flow direction is caused by excess back pressure on the compressor. As the power demand rises from steady state base load to full load in a short time period, the turbine inlet temperature (TIT) increases so that the GT could meet the power demand. Thus, the mass flow rate decreases due to the lower density of hot gas at the turbine inlet. However, the mass flow from the compressor persists causing a pressure buildup at the turbine inlet, increasing the local pressure. As a result of this pressure build up in the compressor outlet, a complete reversal of flow in the impellers can occur, which is called deep surge, and/or an oscillatory flow rate could occur in the impellers that is called mild surge. Figure 1 shows the mechanism of stall/surge in a compressor due to the increase in TIT [17].

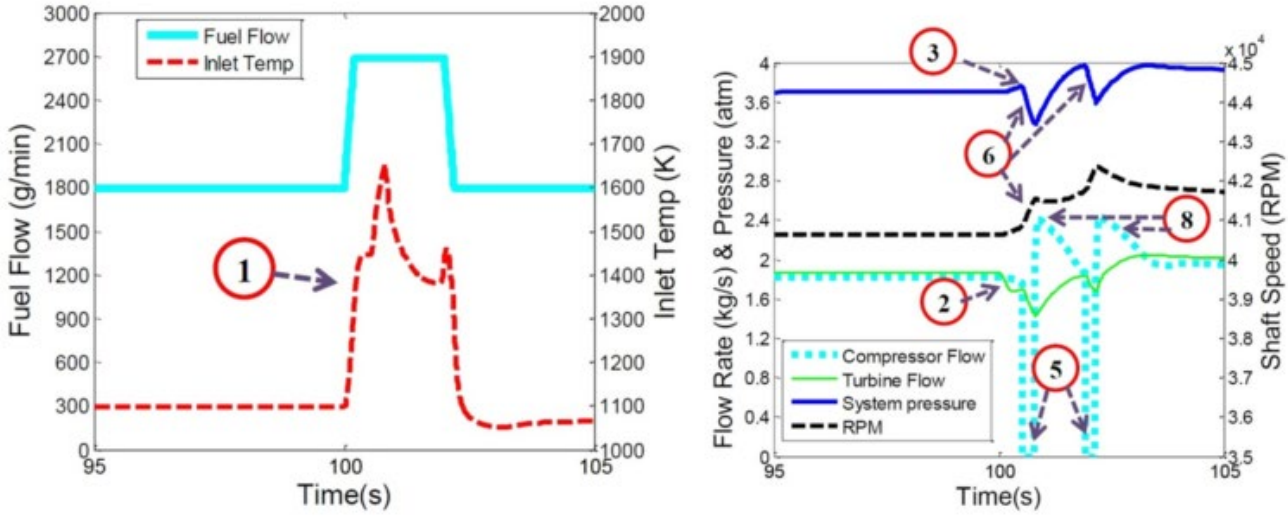

Figure 1. Surge Dynamics in Hybrid SOFC-GT System [17].

The series of operating points that result in a surge event are collectively grouped into the "surge line" that is plotted on compressor maps. These surge events are often followed by compressor stall and highly dynamic, and stressful compressor conditions that can cause a complete mechanical failure of the GT and consequently the hybrid system.

Researchers at the National Energy Technology Laboratory showed the benefits of compressor bleed and cold air bypass for controlling compressor mass flow during transient behavior [27]. Ferrari et al. designed and installed a SOFC-GT physical emulator in the framework of the European Integrated Project [4]. The focus of the study was to minimize the viscous pressure loss to: 1) reduce the unbalance between the compressor and the expander, 2) maintain an accurate measurement, and 3) have an effective plant efficiency. A modular high temperature volume was designed using the CFD tools to achieve a high uniformity in the flow distribution inside the volume and to minimize the pressure losses.

The report concluded that surge occurred during the shutdown for a particular configuration. In another study, strategies to avoid surge or excessive stress during the start-up and shutdown phases were proposed [5]. Dustin McLarty studied the dynamic operation of an SOFC-GT topping cycle and showed that the pressurized hybrid topping cycles exhibit increased stall/surge characteristics particularly during off-design operation [15] [16]. Christoph Stiller suggested that specific incidents should be avoided for safe operation of hybrid systems [25]. Some of these incidents are: compressor stall/surge or cell degradation due to thermal cracking or high temperatures, carbon deposition and anode compartment blocking, and backflow of gas from the burner to the anode cycle, exposing the

anode to oxygen. In this study, a new control strategy for managing the valve was used to generate the requested volume inlet temperature ramp during the hybrid system start-up and shutdown emulation.Compressor performance in GTs is limited by two main lines that are typically plotted on compressor maps: 1) a choke line at high air flow rate and, 2) a surge line at low air flow rate. The surge limit depends upon the system configuration and especially upon the pressure dynamics downstream of the compressor, which dynamics are significantly affected by introducing a fuel cell in place of a combustor, making it difficult to predict surge. Figure 2 presents a typical compressor map with choke and surge limit lines. Reaching the surge limit might reduce the compressor performance temporarily or permanently, as discussed above. Therefore, control strategies are needed to keep the compressor performance in a safe surge margin.

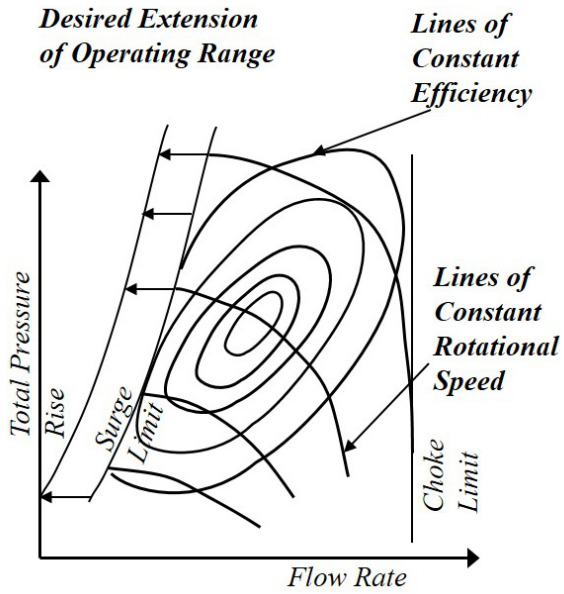

Figure 2. Surge Margin in Compressor Map.

There are two kinds of stall/surge that are common in industrial compressors, which are labeled “deep surge” and “mild surge.” Deep surge is the result of complete reversal of flow in the compressor impeller at a specific time. This type of surge significantly reduces the compressor performance, which could result in complete system failure. The other more common type of the compressor surge is mild surge which is characterized by an oscillatory mass flow rate at the impeller inlet, and outlet caused by partial reversal of flow which causes reduced performance and efficiency of the compressor. However, mild surge is not as severe as deep surge. Figure 3 demonstrates these two common types of compressor surge in industrial compressors.

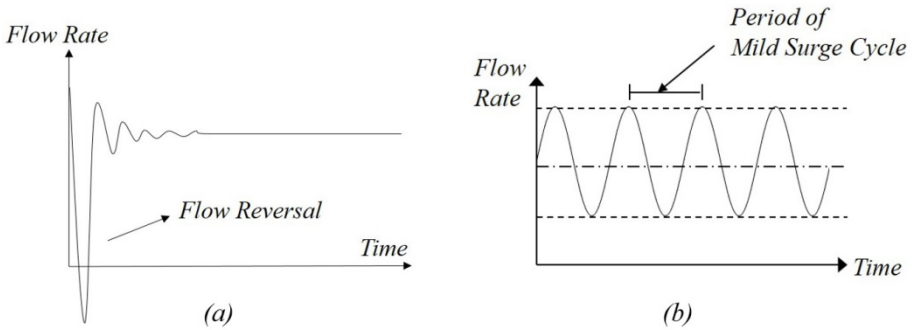

Figure 3. Deep Surge and Mild Surge in a Compressor.

1.2 Objectives

This research addresses compressor stall/surge, one of the most significant challenges corresponding to commercialization of hybrid SOFC-GT system. One of the causes of compressor surge/stall in the hybrid SOFC-GT system is turbine inlet temperature rise due to the transient increase in power demand in a small period of time. One objective of this study is to address this issue by modeling one of the appropriate industrial compressors (i.e., that associated with the 200 kW Capstone micro gas turbine) using CFD tools. In addition, the sizing for the main components in the balance of plant (BOP) for a full-scale 4 MW hybrid SOFC-GT system, using our MATLAB/Simulink dynamic system platform was investigated. A new MATLAB code is developed for each of the components in the BOP, which is basically the conversion of the previous Simulink code developed at NFCRC. It is believed that the new MATLAB code has a better user interface and ease of access than the Simulink code.

1.3 Overall Approach

The overall approach of this research consists of dynamics modeling of the hybrid SOFC-GT system in MATLAB/Simulink software to solve the nodal turbine inlet pressure, followed by 200 kW Capstone single-stage compressor CFD modeling that captures the fluid pressure throughout the compressor impellers to validate the compressor operation feasibility in the hybrid SOFC-GT system. Also, a schematic of the 4 MW system sizing and feasibility is provided to be compared with the actual size of the GE locomotive.

1.4 Scope

This report covers the dynamic analysis of single-stage 200 kW C-200 Capstone micro gas turbine compressor in hybrid FC-GT engine of locomotive due to the step load change in the power demand. It should be noted that this analysis is based on the known locomotive engine power requirements and rotor speed (revolutions per minute [RPM]). Thus, the number of passengers and the elevation profile of the rail route have not been included in this dynamic analysis. However, dynamic response of the compressor due to the step change of power, which was used in previous hybrid FC-GT system studies specifically for locomotive application, was analyzed to address the stall/surge phenomenon and considered as one of the significant challenges in hybrid FC-GT system control. The research applies computational fluid mechanics tools so that it can predict the hybrid system failure as the system operated in transient mode due to the system step power demand change. Prediction of dynamic system behavior near failure mode is the first step in implementation of a hybrid FC-GT system for locomotives.

1.5 Organization of the Report

Section 2 discusses the development of the solid oxide fuel cell model used in the research to investigate SOFC-GT for locomotive applications. The method used to develop the model and simulations executed are outlined in this section followed by results of the simulation. This section continues with a discussion of the development of the computer model and simulation of the full SOFC-GT system based on Bloom Energy and Versa Power fuel cell systems. The results of the simulations based on Bloom Energy and Versa Power are included at the end of the section. Sections 3 and 4 discuss sizing of the SOFC-GT for locomotive applications, and a brief review of solid oxide fuel cell hybrid reciprocating engine, respectively. Finally, Section 5 concludes the research.

2. Modeling Approach

This section explains some of the main concepts related to the SOFC-GT hybrid plant that is studied for dynamic simulation and CFD modeling. The plant consists of the main components of a compressor, a turbine, a SOFC, several bypasses, mixers and heat exchangers. For more discussion about dynamic modeling of this plant, please see [15] [16].

2.1 Developed Hybrid System Model at NFCRC

Figure 4 shows the model of 4 MW power generation hybrid system has been previously developed at NFCRC at UCI using MATLAB/Simulink software. This model was used to show that such systems, when properly designed and controlled, can have higher efficiency than the previously tested SOFC-GT systems. The model consists of a compressor, a turbine, a blower, a SOFC, a combustor and three mixers, as shown in Figure 5. This model has been previously studied for different applications of the hybrid SOFC-GT system by Brouwer et al. [14] [15] [16] [17]. The model includes one fuel cell bypass and several heater bypasses.

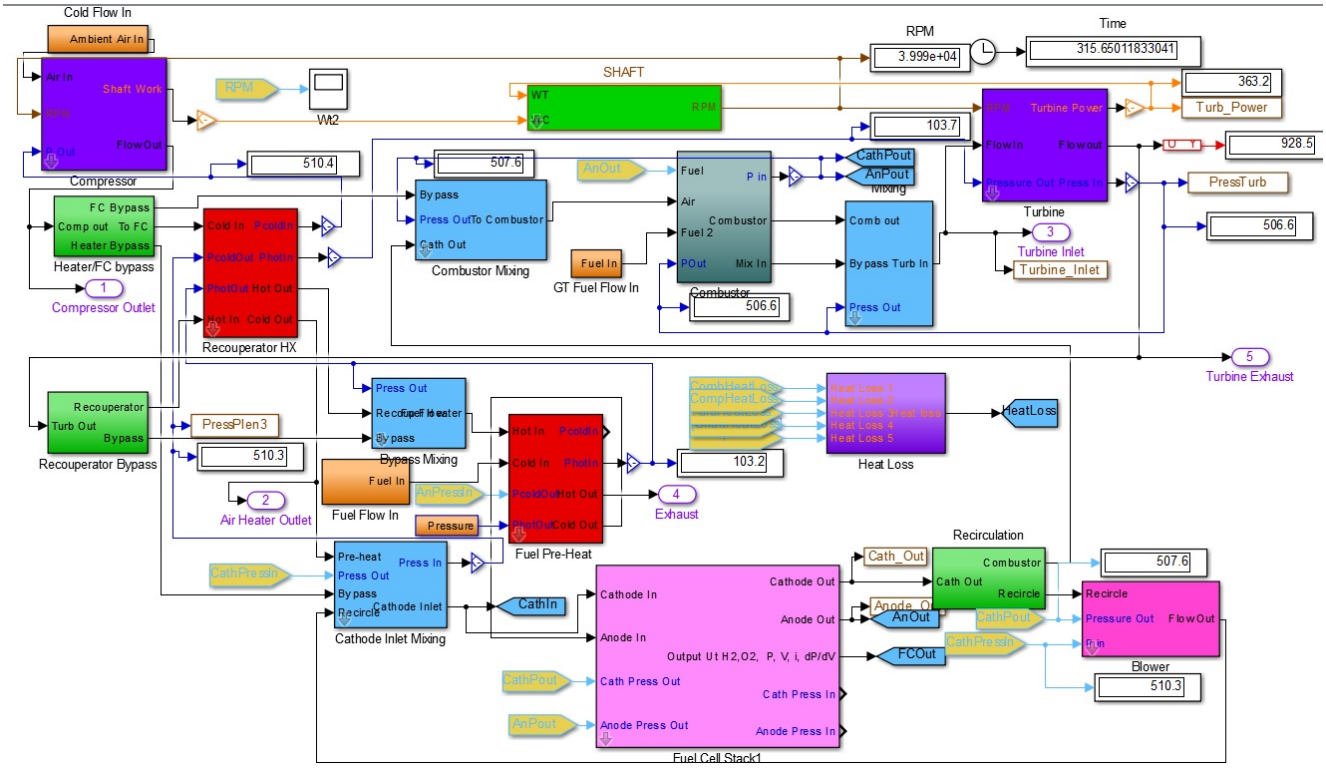

Figure 4. SOFC-GT BOP Locomotive System.

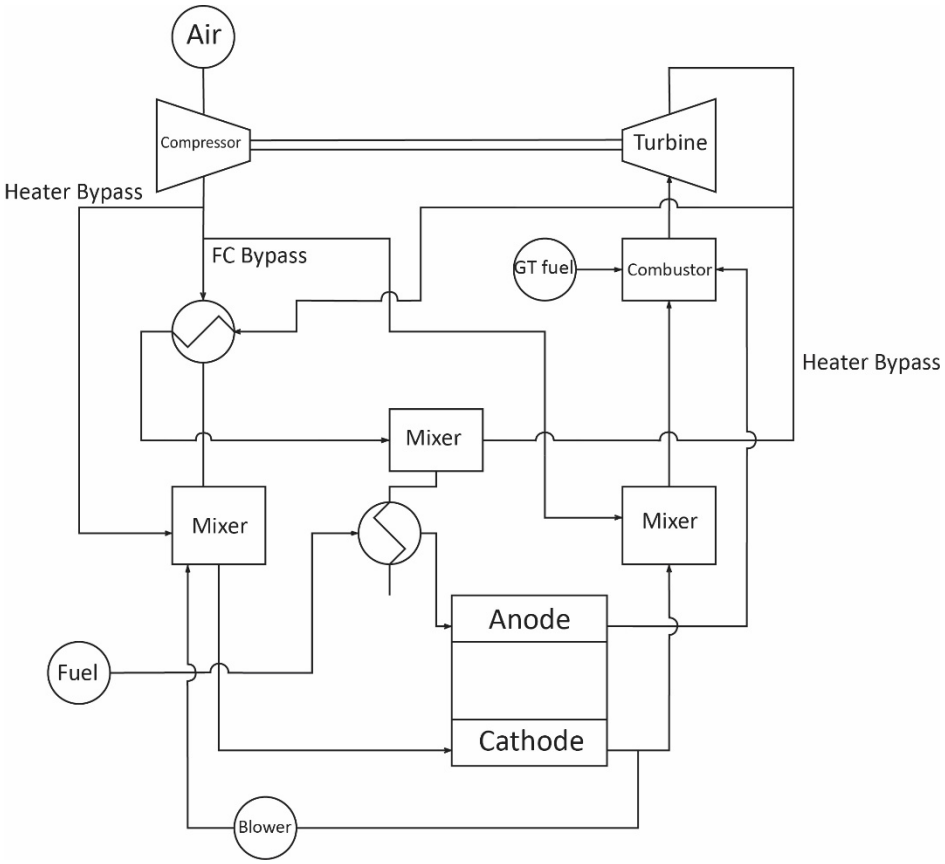

Figure 5. Hybrid SOFC-GT Locomotive Engine.

2.2 Solid Oxide Fuel Cell Modeling

The reversible potential is calculated from the Eq. (1):

$$E_r = E^\circ + \Delta E = \frac{-\Delta G^\circ}{nF} + \frac{-\Delta G}{nF} = \frac{-\Delta G^\circ}{nF} + \frac{RT}{2F}\ln\frac{P_{H_2}P_{O_2}^{\frac{1}{2}}}{P_{H_2O}} \quad (1)$$

To reach a high reversible voltage, the hydrogen and oxygen partial pressures have to be high enough and the steam partial pressure has to be low. The irreversible losses are: 1) Activation overpotential (η_{act}), 2) Ohmic overpotential (η_{Ohm}) and 3) Concentration overpotential (η_{Conc}). Hence, the actual potential of the cell is described in the form of Eq.(2):

$$E = E_r - (\eta_{act} + \eta_{Ohm} + \eta_{Conc}) \quad (2)$$

2.2.2 Reformer Model

For a natural gas fed hybrid SOFC-GT system, either an internal or external reformer can be integrated in the system. To decrease the expense of an external reformer and to provide additional cooling for SOFC stack, internal reformer is preferred over external reformer. The reforming equations and the available hydrogen for the stack are in the form on Eq. (3) to Eq. (6):

$$Reforming: CH_4 + H_2O \leftrightarrow CO + 3H_2 \quad (3)$$

$$Shifting: CO + H_2O \leftrightarrow CO_2 + H_2 \tag{4}$$

$$Electrochemical: H_2 + \frac{1}{2}O_2 \rightarrow H_2O \tag{5}$$

$$H_{2,avail} = \dot{n}_{fuel} \times (4X_{CH_4} + X_{CO} + X_{H_2}) \tag{6}$$

2.2.3 Turbomachinery

Shaft speed, pressure ratio and flow rate were normalized using Eq. (7) to (9):

$$N_{RPM} = \frac{RPM}{\sqrt{\frac{T_{stag}}{T_d es}}.RPM_{des}} \tag{7}$$

$$N_{Flow} = \frac{Flow}{Flow_{des}}.\frac{\sqrt{\frac{T_{stag}}{T_{des}}}}{\frac{P_{in}}{P_{des}}} \tag{8}$$

$$PR = \frac{P_{out}}{P_{in}.PR_{des}} \tag{9}$$

Where, the parameters were defined using the Eq. (10) to Eq. (13):

$$Stagnationtemperature: T_{stag} = T_{in}.(1 + M^2(\frac{\gamma - 1}{2})) \tag{10}$$

$$MachNumber: M^2 = \frac{R_u \gamma T_{in}}{MV_{in}} \tag{11}$$

$$Velocity: V_{in} = \frac{\dot{n} R_u T_{in}}{A_{in} P_{in}} \tag{12}$$

$$Specificgasconstant: \gamma = \frac{C_p}{C_v} = \frac{C_p}{C_p - R} \tag{13}$$

The input parameters for the compressor were the ambient temperature, the species concentrations, the shaft speed, and the inlet/exit pressures. The ambient air pressure was assigned to the inlet pressure. The outlet pressure was found by backward solving of the pressure loss through the other components of the system. Alternatively, it could be solved by defining a node at the outlet of the compressor and solving the mass balance for the nodes. Two conservation of energy models were considered for the compressor [9]. The first consisted of the working fluid and the second included the compressor solid mass demonstrated in Eq. (14) and (15).

$$\frac{dT_g}{dt} = \frac{\dot{W}_C + (h.\dot{n})_{out} + h_c A_{sur}(T_s - T_g)}{C_p . \frac{P_{out} V}{R_U T_g}} \tag{14}$$

$$\frac{dT_s}{dt} = \frac{h_c A_{sur}(T_g - T_s) + \varepsilon\sigma A_{sur}(T_{amb}^4 - T_s^4)}{C_p . m} \tag{15}$$

2.2.4 Fluid Mechanics Problem in Hybrid SOFC-GT Systems

The schematic of the fluid mechanics problem that is solved in this research is shown in Figure 6. The plenum chamber resembles the diffuser between the two impellers. Deep surge is the phenomenon when the pressure at the plenum is high enough that it could result in a complete reversal of the flow in the impeller. The diffuser between the plenum volume resembles the diffuser section, for the first impeller, while the plenum volume for the second impeller is replaced by the simulated pressure variation over time.

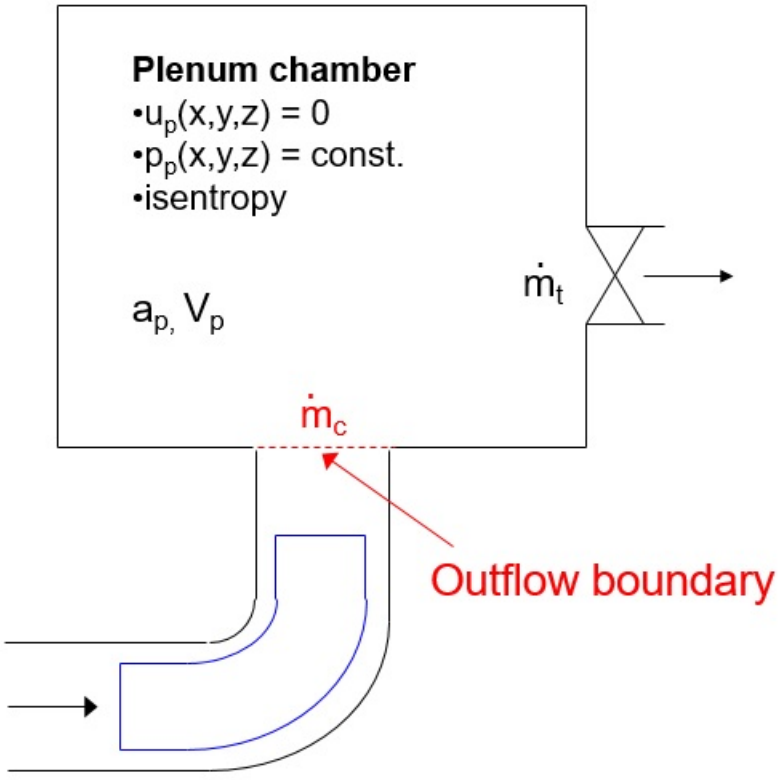

Figure 6. Schematics of Plenum at the Inlet of Turbine.

Eq. (16) explains the pressure gradient of the plenum over time. The equation expresses the conservation of mass and isentropic expression for speed of sound:

$$\frac{dP_p}{dt} = \frac{a_p^2}{V_P}(\dot{m}_c - \dot{m}_t) \tag{16}$$

Where, a_p is speed of sound and V_p is the volume of the plenum.

2.3 Applied Control Algorithms

The control modeling approach couples a simplified dynamic model for determining the hybrid system and compressor exit pressure dynamics that are supplied to a CFD approach for resolving the fluid flow through the compressor. The dynamic system model uses a simplified geometrical representation of the SOFC integrated into the system with heat exchangers, a reformer, and a steady-state GT compressor and turbine map with a large volume between them that can accumulate mass and produce appropriate pressure dynamics during dynamic operation of the hybrid system.

The approach is patterned after that previously developed at the NFCRC [14, 15, 16, 17]. Figure 6 shows the control system applied to the hybrid SOFC-GT system consisting of five controllers. Figure 7 shows the power demand and the power generated by the SOFC stack and the GT over a 10,000 second time range. The SOFC stack and the GT generate 2.2 MW and 800 kW nominal power respectively, at steady state conditions. After the hybrid system reached a steady state operation, several step power demand changes (up and down) were applied to the system model as shown in Figure 7.

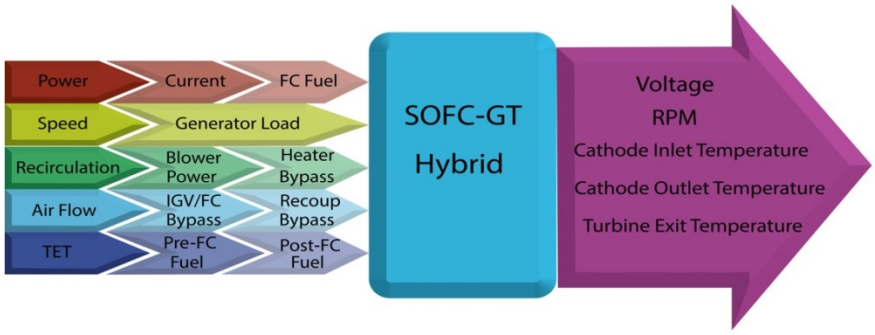

Figure 7. Control Algorithm of Synchronous SOFC-GT Topping Cycle [17].

Table 2. SOFC-GT Hybrid System Controller Specifications [17].

State	*Actuator*	*Integral Gain*	*Proportional Gain*	*Feed-forward gain*
Net Power	Current	1×10^{-2}	0	0
Turbine Speed	Generator Load	5×10^{-1}	1×10^{-2}	0
Cathode Inlet Temperature	Blower Power/ Heater Bypass	5×10^{-2}	4	0
Cathode Exhaust Temperature	IGV angle or FC bypass/Recuperator bypass	0 (IGV) & 10^{-3} (FC bypass)	1 (IGV) & 2 (FC bypass)	0.7 (IGV) & 1.16 (FC bypass)
Turbine Exhaust Temperature	Pre-fuel cell fuel r Post-fuel cell fuel	5×10^{-2} (Pre) & 10^{-4} (Post)	0	0

The combined approach with feed-forward control applied to the hybrid model enables rapid load following at high efficiency. This control method was validated using the UCI campus demand profile. Figure 8 demonstrates the power demand for the 268 kW Bloom Energy SOFC system that is applied to the newly developed MATLAB code. Figure 9 shows the pressure dynamics response of the dynamic model to step power demand change in 200 kW C-200 Capstone micro gas turbine.

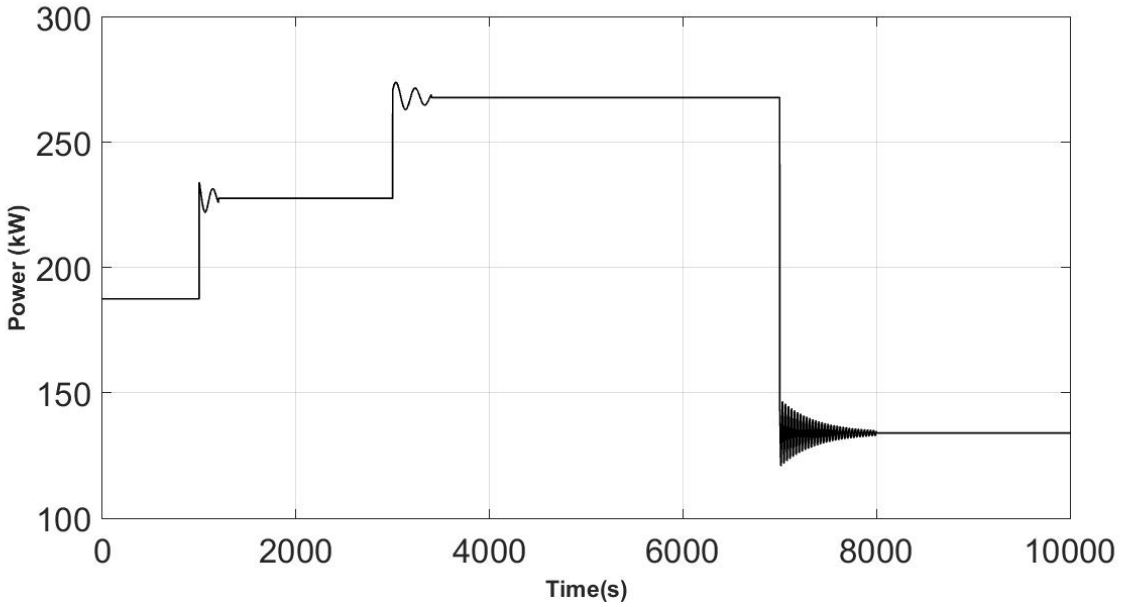

Figure 8. Power Demand Profile Applied To Bloom Energy 268 kW SOFC System.

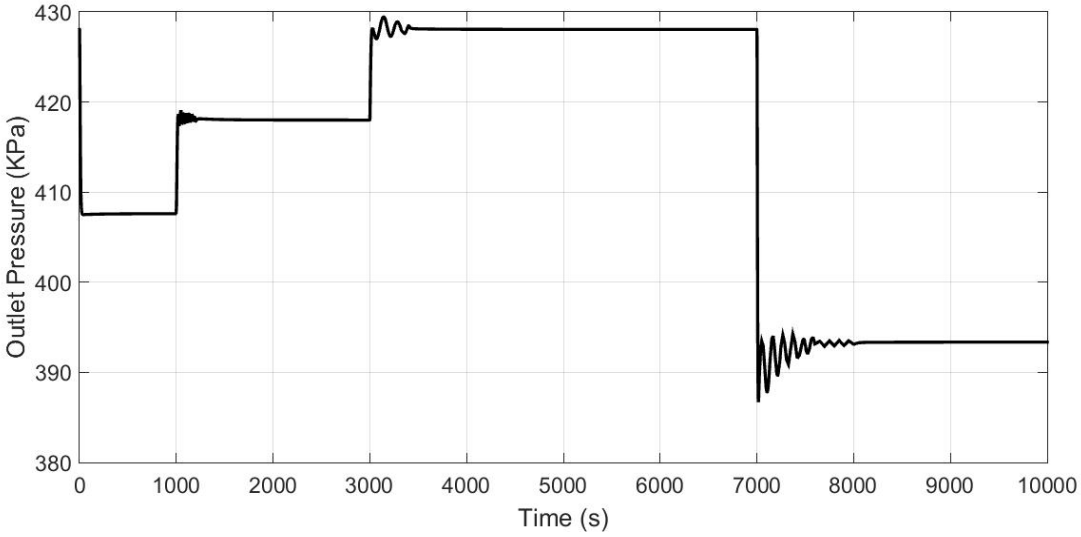

Figure 9. Pressure Response of the Step Power Change of the Dynamic Model to the C-200 Capstone Micro Gas Turbine.

2.4 CFD Simulation

In this study, CFD modeling is used to explore and understand surge phenomenon in the hybrid FC-GT system. CFD analysis is used on single-stage compressor configuration and its feasibility in the hybrid locomotive test system during the dynamic operation is investigated. The conceptual design of compressor is based upon the GTs manufactured by the C-200 Capstone micro gas turbine. The single-stage compressor design as shown in Figure 10 below has a similar design of that used in the C-200 [9]. The air mass flow rate and the design parameter (RPM) has been changed to match C-200 design conditions as required for the 500 kW hybrid test system. Figure 11 shows a cross-section of the C-200 micro gas turbine system. Table 4 shows the performance characterization of the 200 kW C-200 Capstone micro gas turbine. In this study, the SOFC-GT model design conditions are calibrated for the 61,000 RPM condition to match up the hybrid FC-GT design operating conditions of the 200 kW C-200. The blades and diffuser are sized for the net 1 kg/s (2.20 lbm/s) air mass flow rate.

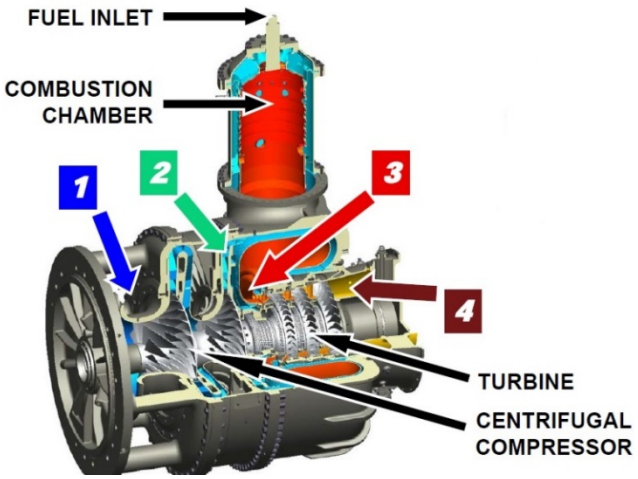

Figure 10. 1.7 MW Kawasaki Gas Turbine for Long Haul Locomotive Hybrid System Engine [9].

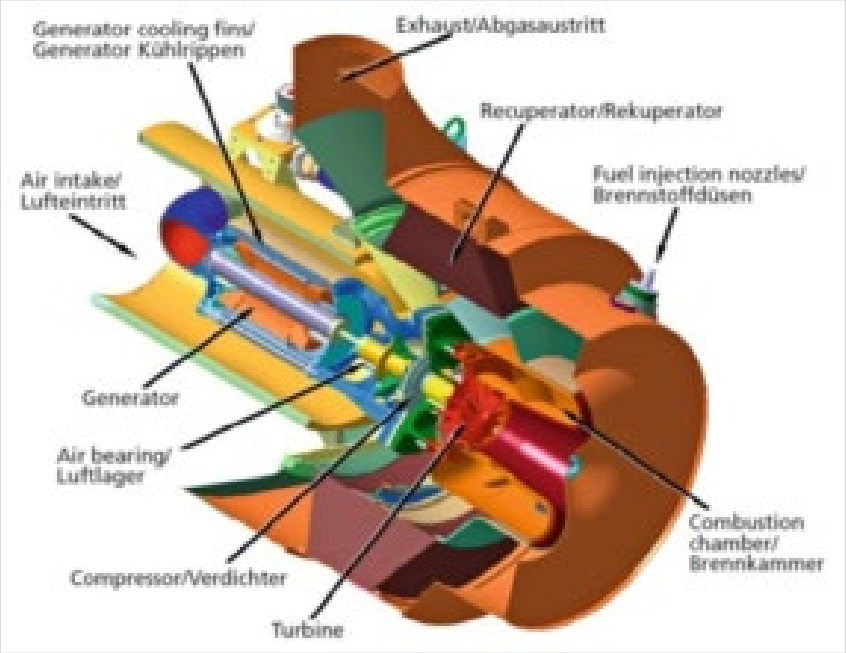

Figure 11. 200 kW Capstone Micro Gas Turbine for Test Locomotive Hybrid System Engine [8].

Table 3. C-200 Captone Micro Gas Turbine Compressor Design Characteristics [9].

Parameter
Single stage centrifugal compressor section
One stage radial turbine section
Short rotor span
Single combustion chamber

Table 4. 200 kW C-200 Capstone Gas Turbine Design Conditions [7].

Parameter	Unit	Value
System Power	kW	200
Design Speed	RPM	61,000
Electrical efficiency	%	33
Pressure Ratio	None	4
Design Flow	kg/s	1

2.4.1 Geometry Modeling

Due to their complex geometry, centrifugal compressors can be difficult systems to analyze using CFD. The configuration considered in this study includes a fast rotating impeller coupled to a stationary diffuser. To simulate the entire compressor stage, two sections (i.e., the rotating impeller and the stationary diffuser) must be modeled together. The impeller blade was designed for an overall pressure ratio of 4 and a rotating speed of 61,000 RPM. The geometry consists of impellers and a diffuser with an inlet connected to the outlet of the diffuser. To reduce the computational costs, full 360 degree symmetrical boundary conditions are used to model one flow passage of the compressor. Each of the rotating and stationary sections were meshed independently. The impellers were meshed by the structured hexahedral method in ANSYS TurboGrid software while the the diffuser was meshed using unstructured tetrahedrals with boundary layer refinements. The three separate mesh grids, were connected by defining a stage averaging interface between the rotor and diffuser sections.

2.4.2 Boundary Conditions

Stage averaging is used as a method of interface connection between the diffuser and impeller. In this method circumferential averaging is applied at the interface between the rotor and stator. To apply correct boundary conditions on the fluid domain, a subsonic uniform air flow rate boundary condition with atmospheric pressure and temperature is applied to the inlet. The turbulent intensity was set to 5 percent. A step load change pressure dynamic perturbation that resulted from the hybrid SOFC-GT system simulation, is applied to the domain outlet. Since the diffuser domain is stationary and the impellers are rotating, an interface boundary is defined between the rotating impeller and the stationary diffuser.

2.4.3 Fluid Dynamics Model

In this study, a fluid dynamic Reynolds Averaged Navier-Stokes (RANS) based model of SST k-ω is used. Using k-ω instead of k-ε allows for better resolution of boundary layers, especially under adverse pressure gradients. However, in the current study, the SST model was more difficult to converge than the k-ε model. The k-ω model is known as the best RANS model for wall bounded aerodynamic flows (e.g., airfoils, compressors, turbines, and flows) with separation due to adverse pressure gradient. In addition, the SST model is used to reduce the boundary condition sensitivity. This model is also known as the best model for heat transfer predictions. In general, SST model, provides more accurate prediction of flow separation than other RANS models. ANSYS CFX was used as a CFD solver for this study. CFX was chosen due to the proven ability to tackle the complex turbomachinery problems faced in the GT industry. To obtain a good convergence, first the solver converged to the steady state solution. Following the stationary solution, the transient boundary condition was applied to the model and solved for the dynamic solution.

2.5 Results

Transient dynamic operation of hybrid FC-GT system components, while maintaining the 500 kW test locomotive power requirements, is analyzed using MATLAB/Simulink software. Figure 12 demonstrates the operating point of this hybrid system which is below the compressor surge line. The total simulation is a time span of 10,000 seconds. The control strategies were developed at NFCRC to prevent the system from operating beyond the surge line. Figure 12 demonstrates that the operating point is below the surge line and in the safe operating region. These implemented control algorithms work well to assure that the compressor will not operate in the deep surge condition, however, real

industrial compressor performance has to be investigated for these same operating conditions in the hybrid system.

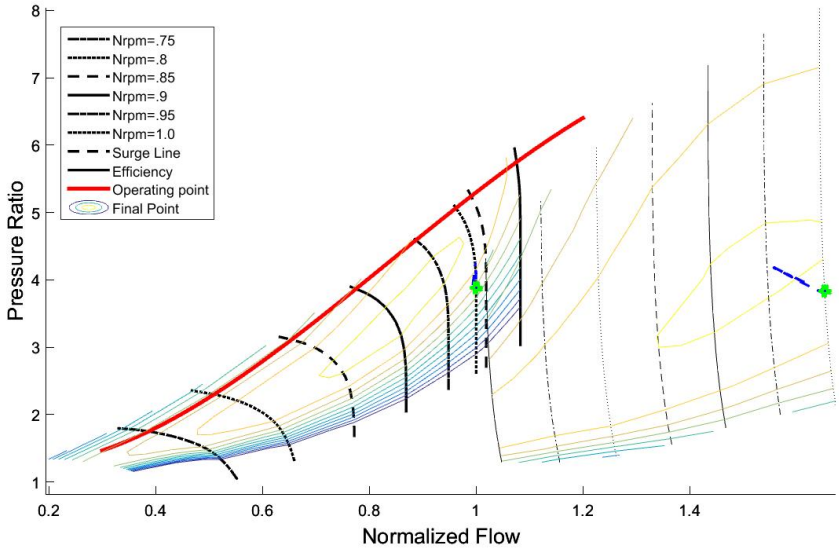

Figure 12. Operating Point of 200 Kw C-200 Micro Gas Turbine At the Time Span of 10,000 s as Operated in a SOFC-GT System Cycle.

The dynamic pressure step perturbation due to the transient load variation in a small time period is applied to the diffuser outlet. This perturbation results in the development of high pressure in the diffuser and impellers as shown in Figure 13 and Figure 14 and as a function of rotor revolution. The pressure at the diffuser outlet reduces over time as the power demand decreases. Low pressure development takes time to be developed on the impeller due to the stabilized flow in the diffuser located right after the impeller. This pressure development took 53 rotor revolutions.

The results would validate the utilization of CFD tools in C-200 and lead to a better understanding of the flow phenomenon within the single-stage centrifugal compressor. Lower pressure on impeller followed by pressure step decrease, results in lower pressure in the diffuser and the first impeller. Ongoing mass flow rate through the impeller and reduction in back presssure on the impeller causes a pressure reduction in the diffuser lowering the risk of surge in the impeller.

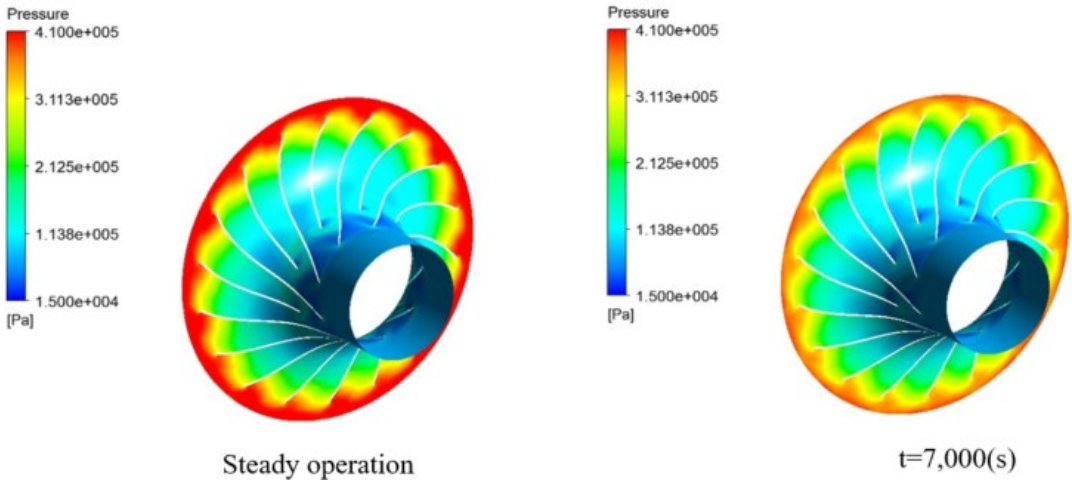

Figure 13. Pressure Distribution on the Impeller at t=7,000 s.

Figure 14, shows that the higher velocity distribution at the impeller is a result of lower pressure in the impeller. Due to the higher velocity, high Mach regions on the leading edge are greatly reduced. However, higher velocities on the trailing edge can be seen. Higher tangential velocity in the impeller outlet is shown that causes higher mass flow rate through the first impeller inlet.

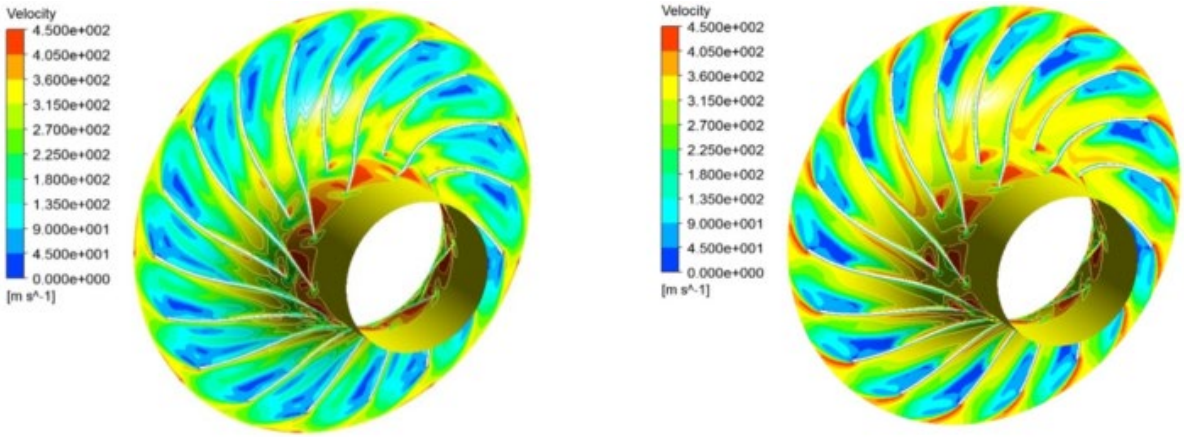

Figure 14. Velocity Contours on the Impeller at t=7,000 s.

Low outlet pressure causes higher air mass flow at the impeller outlet. In addition, due to the low pressure, temporary higher velocitiy region develops in flow direction from the impeller inlet toward the leading edge. As a result, vortices previously formed on the blades are reduced resulting in an increased impeller compression efficiency.

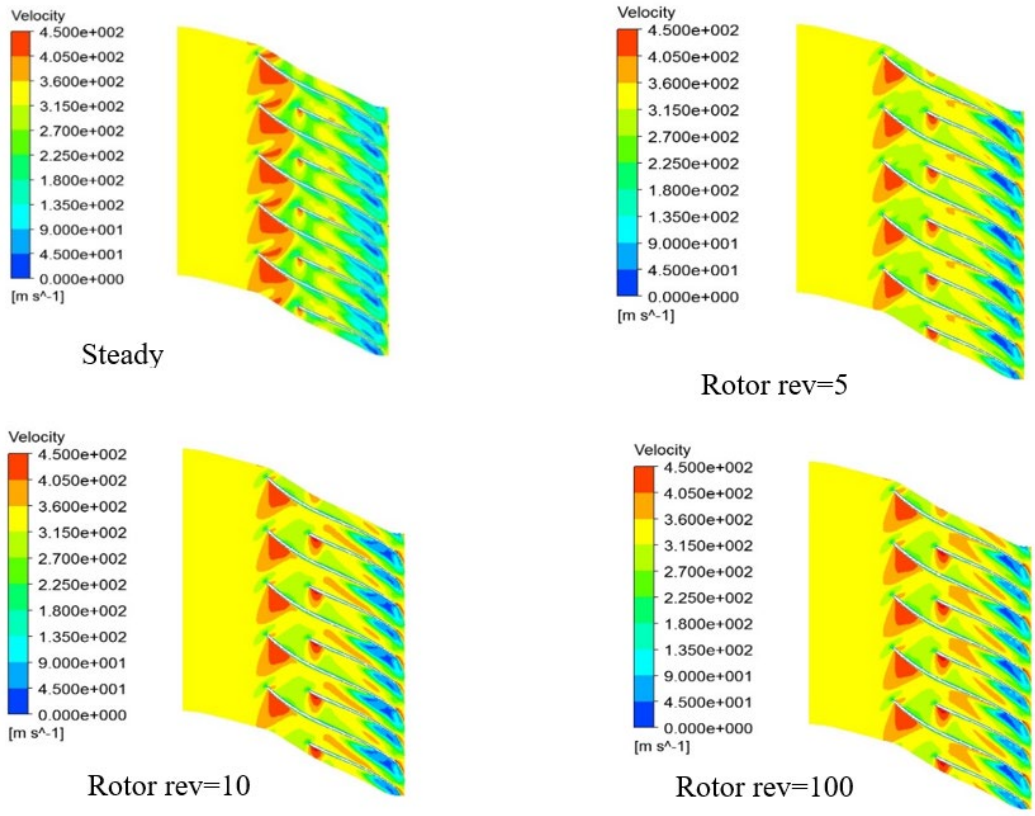

Figure 15. Velocity Development on the Impeller Blades at t=7,000 s.

Figure 14 shows the evolution of the velocity over the impeller blades as the rotor spins. Figure 16 shows the velocity vectors on the impeller inlet over time. Comparing these figures, it is evident that the net mass flow rate of air is consistent over time, showing a sustained flow rate during the sudden power demand reduction. In addition, high volume of the diffuser plays a significant role stabilizing the flow at the impeller inlet. Thus, whenever fast transient power demand is required, the diffuser delays the surge on the impeller and reaches normal operation before the second surge begins.

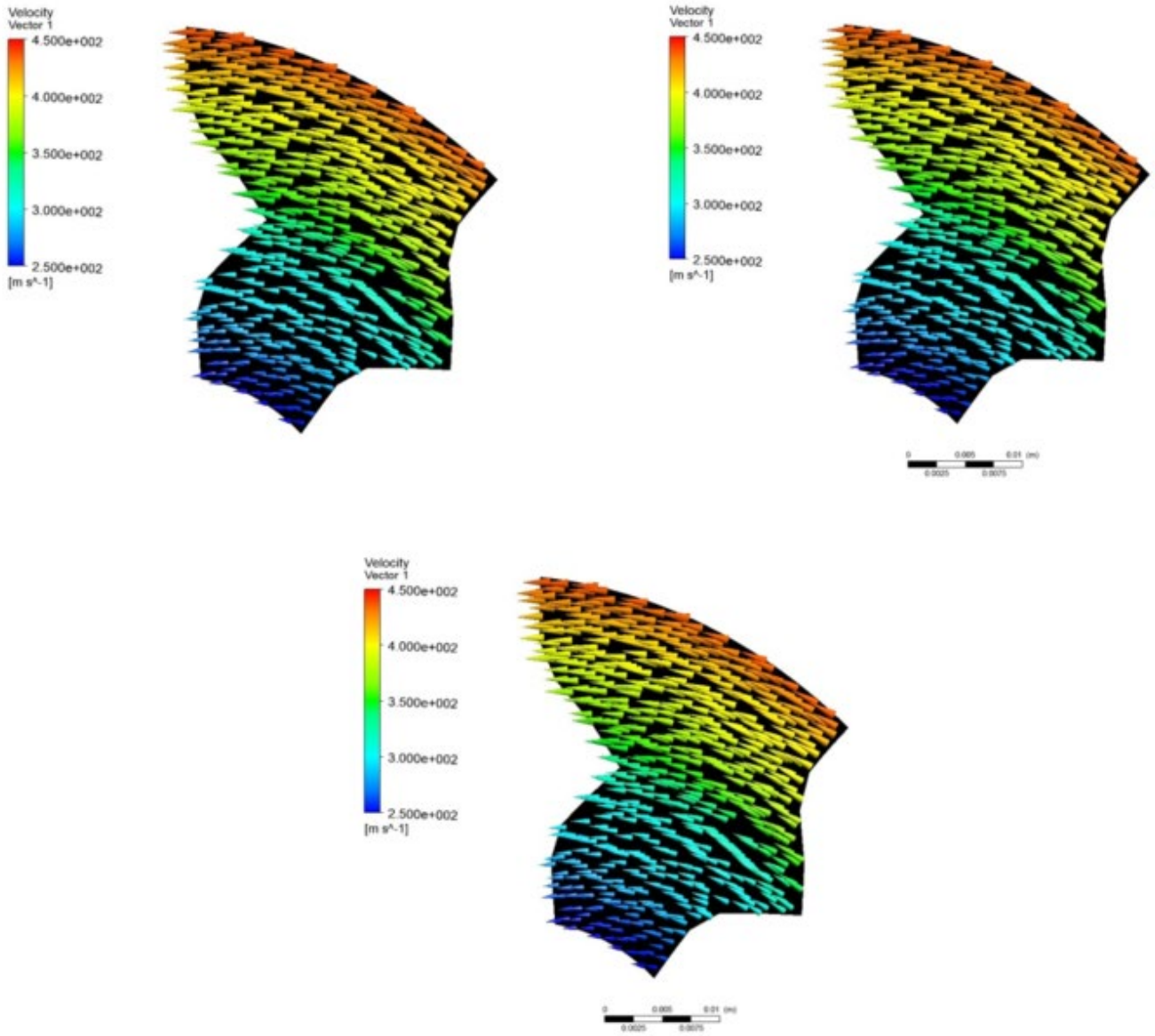

Figure 16. Velocity Vectors on the Impeller Inlet.

Figure 17 shows the pressure development throughout the diffuser over time. It could be seen that the pressure reduces significantly due to the reduction in power demand reducing the surge risk in the impeller. Stable flow in the diffuser plays an important role in reduction of back pressure on the impeller and keeps the air mass flow rate at a desirable level of 1 kg/s (2.20 lbm/s).

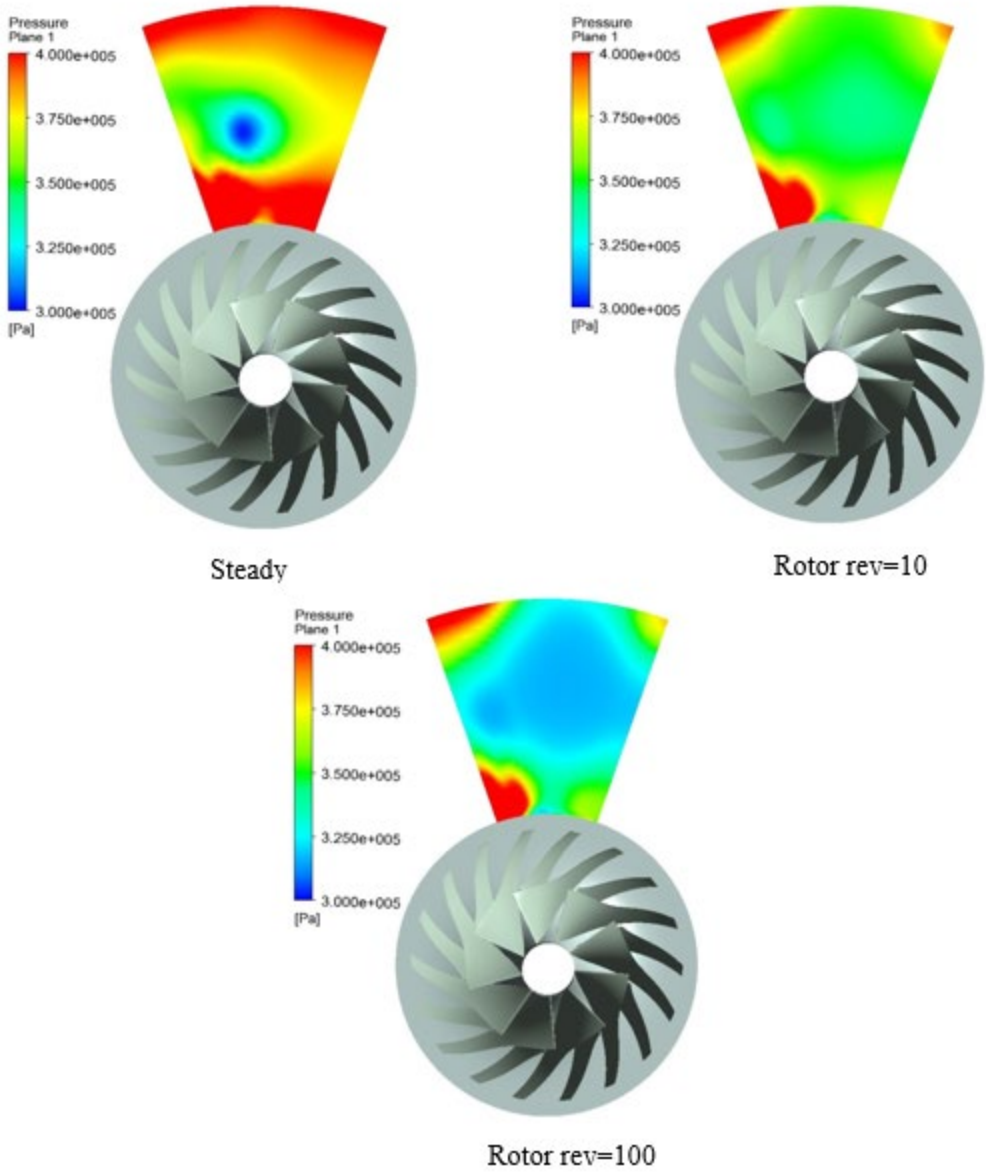

Figure 17. **Pressure Reduction in the Diffuser Connected to the Impeller Outlet at t=7,000 s.**

Figure 18 demonstrates the mass flow rate oscillation corresponding to the mild surge on the impellers outlet, showing a sustained flow rate in C-200 compressor during the hybrid SOFC-GT operation. During this time, the radial velocity at the impeller outlet increases and the mass flow rate through the outlet increases, reducing the surge risk in the C-200.

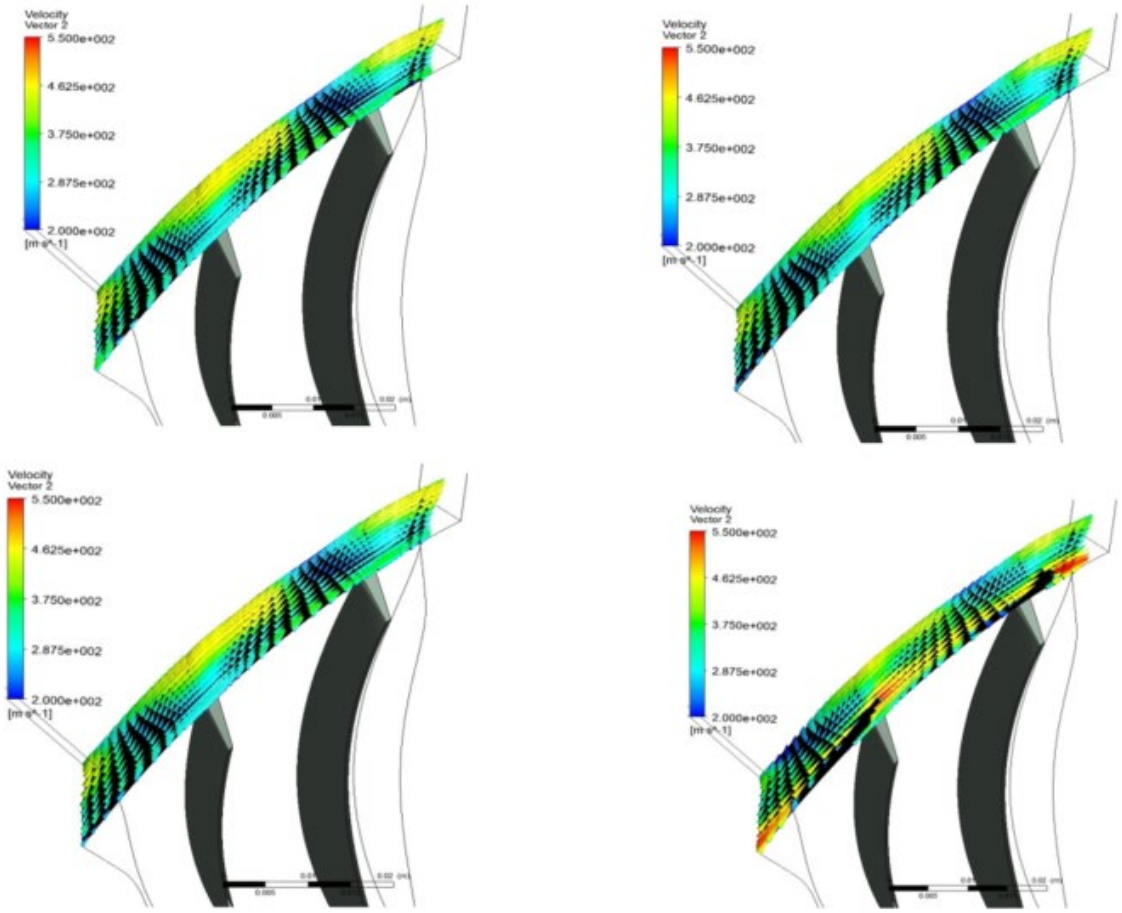

Figure 18. Impeller Outlet Velocity and Flow Rate Increase at t=7,000 s.

Figure 19 show the velocity profile over the impeller at time=3000 s, when the power demand increases step wise to 200 kW. This is a more critical case than the previous case as the pressure increases due to power increase. It is evident that the velocity is greatly reduced, which lowers the net mass flow rate.

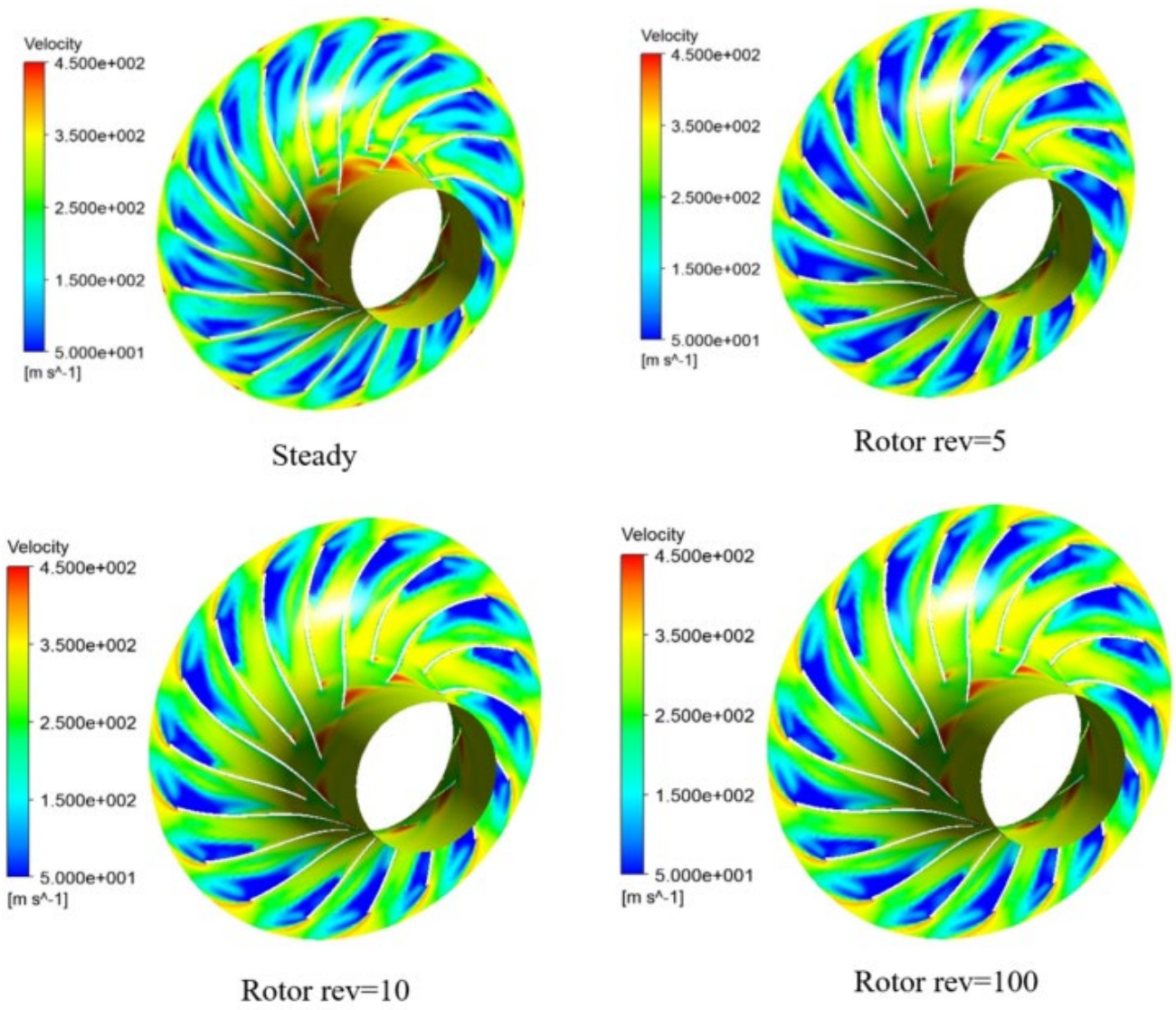

Figure 19. Velocity Reduction on the impeller at t=3,000 s.

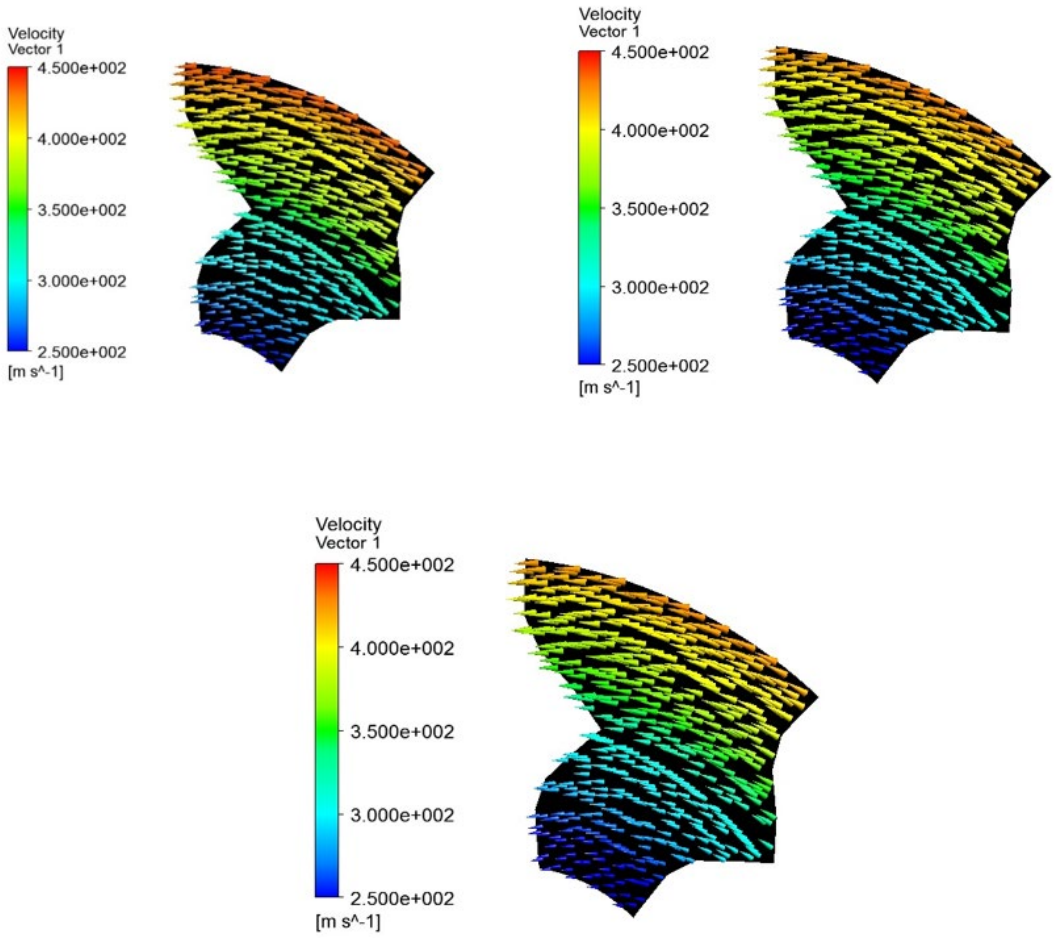

Figure 20. Velocity Vectors on the Impeller Inlet at t=3,000 s.

Figure 20 shows the velocity region on the impeller blades. As the pressure increases, the velocity decreases significantly on the trailing edge. However, after 20 rotor revolutions, the velocity reaches to constant value, resulting in a sustained mass flow rate. High vorticity region that was formed at 5 rotor revolution, diminishes on the trailing edge after 20 rotor revolutions.

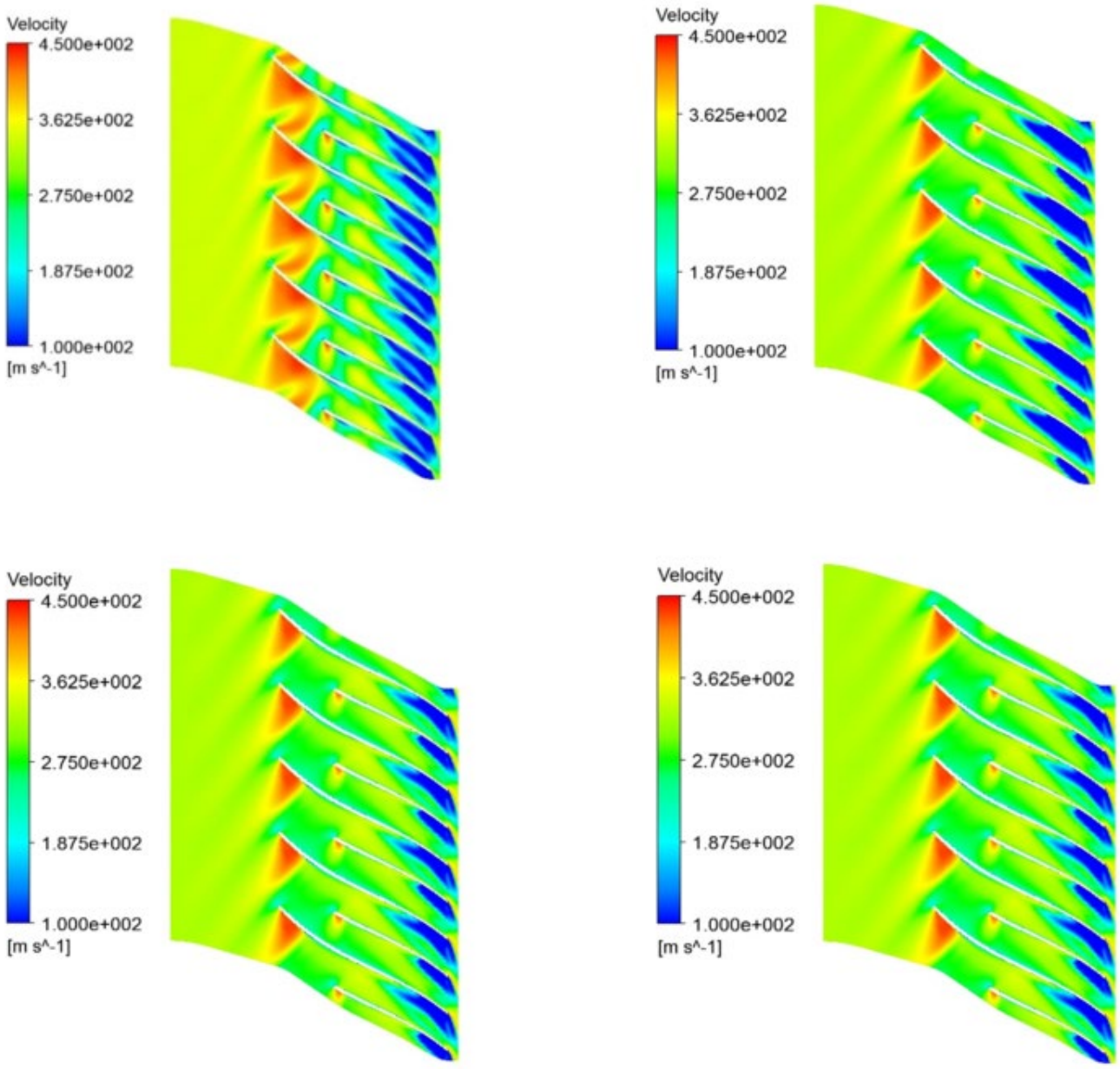

Figure 21. First Impeller Velocity Distribution from Leading Edge to Trailing Edge.

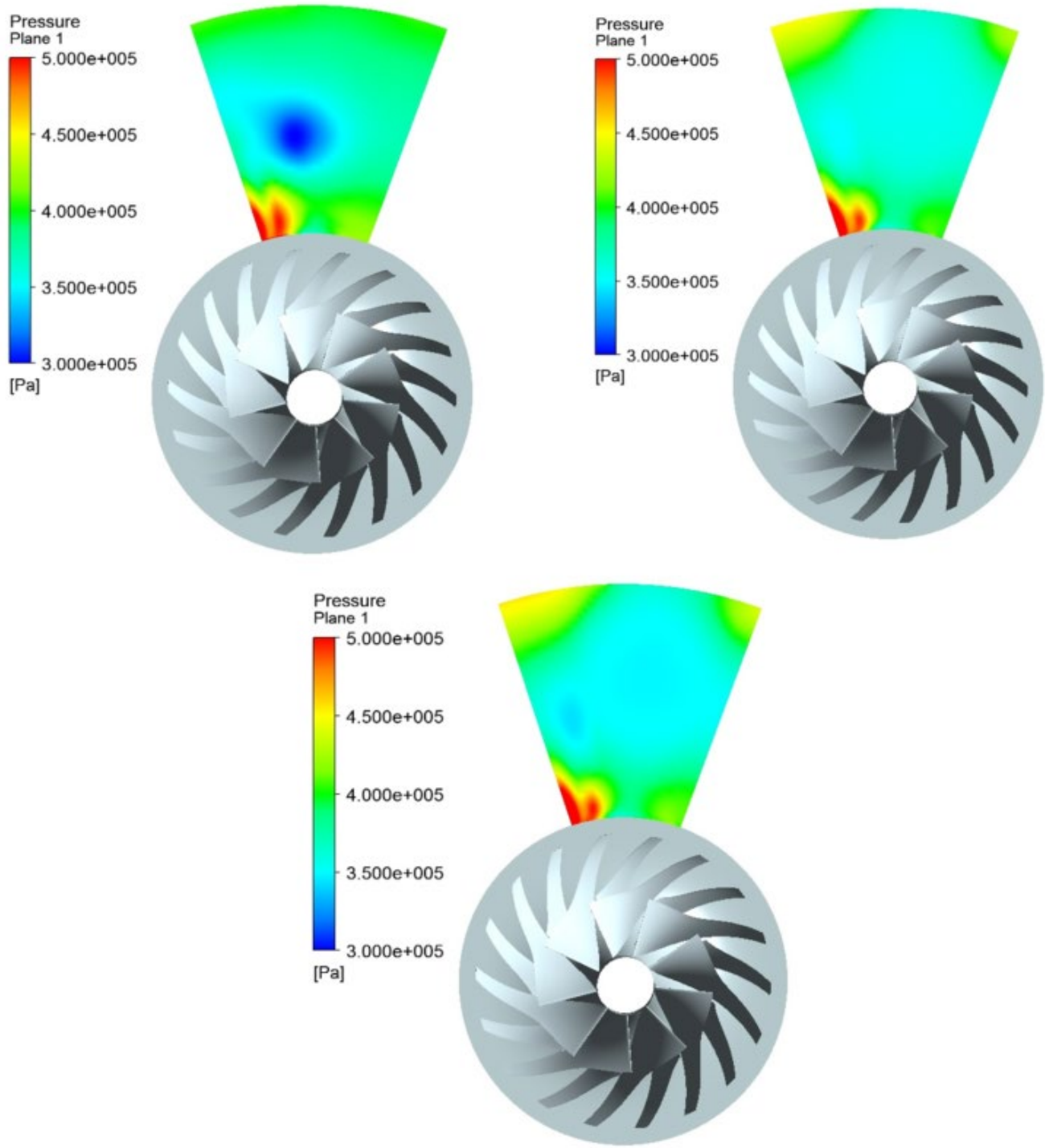

Figure 22. Pressure Increase at t=3,000 s on the Impeller Due to the Increase in the Power Demand.

Figure 23 shows that as the outlet pressure increases, the flow velocity on the impeller at the trailing edge gradually decreases. This situation is accompanied by the vortices formed along the blades and the splitters. Development of control algorithms are necessary to prevent the local high velocity on the blades.

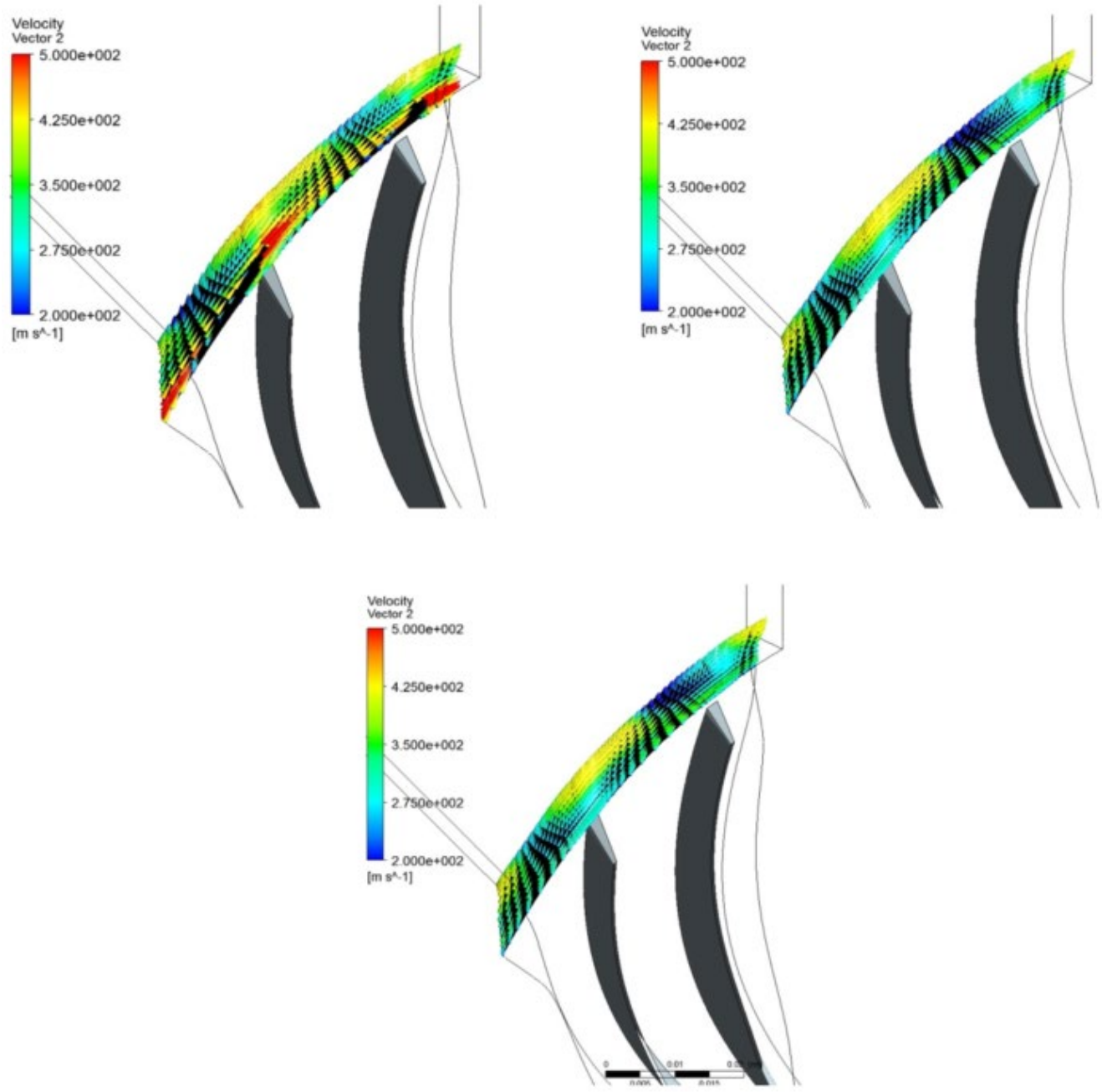

Figure 23. Impeller Outlet Velocity Reduction at t=3,000 s.

2.5.1 Surge Analysis Results

The calculated values of mass flow rate at different parts of the single-stage C-200 compressor are shown in Figure 24, Figure 25, Figure 26, and Figure 27 as a function of the rotor revolutions for two times of t=3000 s and t=7000 s. The dynamics of the pressure increases in both impellers are shown in Figure 28. Note that, in the single-stage configuration studied in this section there is a net and sustained mass flow rate through the compressor outlet after the pressure step is relaxed to a constant value.

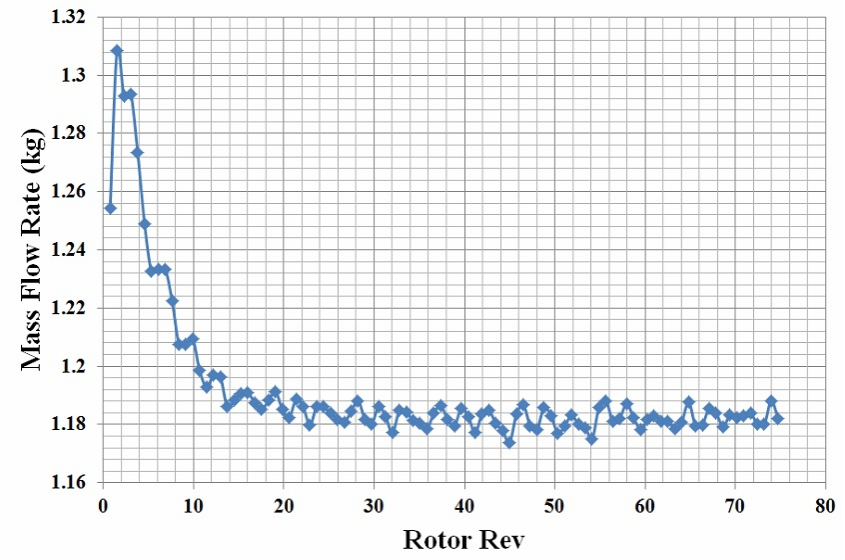

Figure 24. Inlet Mass Flow Rate through the Impeller at t=7,000 s.

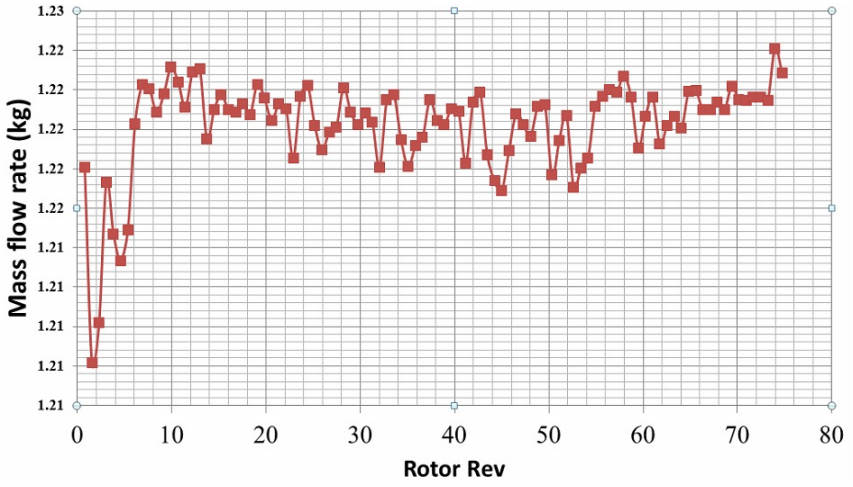

Figure 25. Impeller Outlet Mass Flow Rate Increase at t=7,000 s.

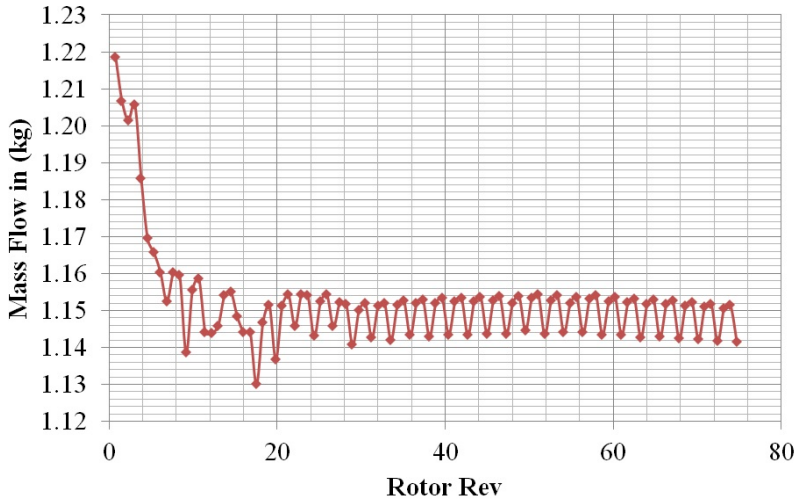

Figure 26. Outlet Mass Flow Rate Reduction in the Impeller at t=3,000 s.

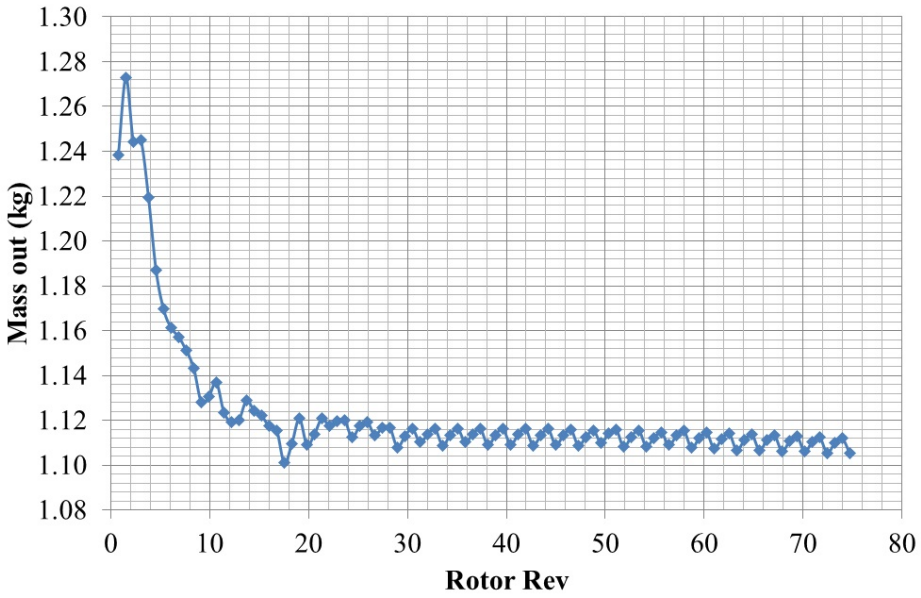

Figure 27. Inlet Mass Flow Rate Reduction in the Impeller Inlet at t=3,000 s.

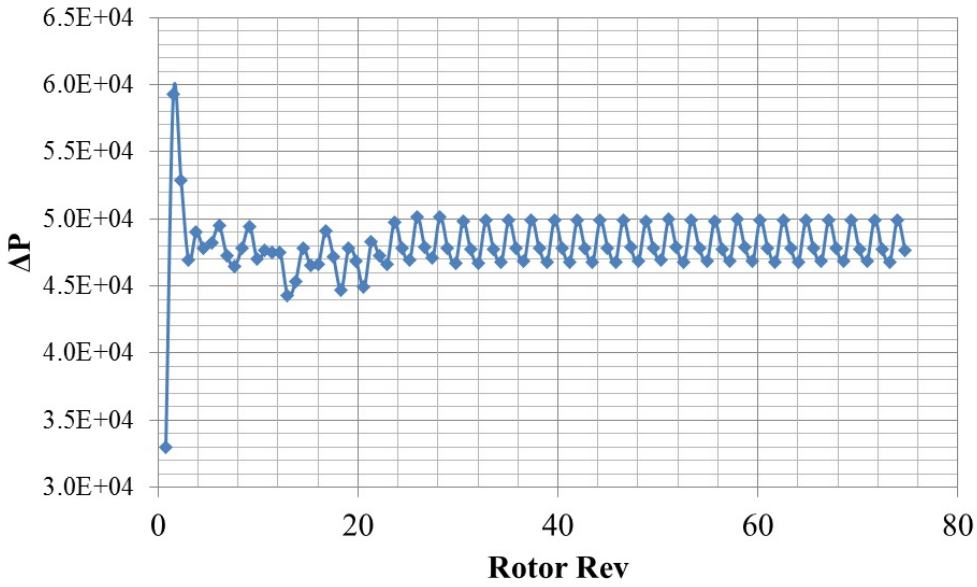

Figure 28. Pressure Build Up in the Impeller and Diffuser at t=3,000 s. Dynamic Operation of Bloom Energy and Versa Power Systems

A MATLAB model is developed for simulation of the hybrid SOFC-GT system. Currently, the fuel cell, gas turbine, and BOP are being developed in this platform. In this section, dynamic simulation of the fuel cell types from Bloom Energy and Versa Power are accomplished.

2.6 268 kW Bloom Energy SOFC system

A step-wise power demand similar to notched locomotive power demand requirements is applied to the Bloom Energy 268 kW system depicted in Figure 29 to investigate the system response. A plot of the power demand of this system over time is shown in Figure 30.

Figure 29. Artist Rendering of a Bloom Energy 268 kW SOFC System.

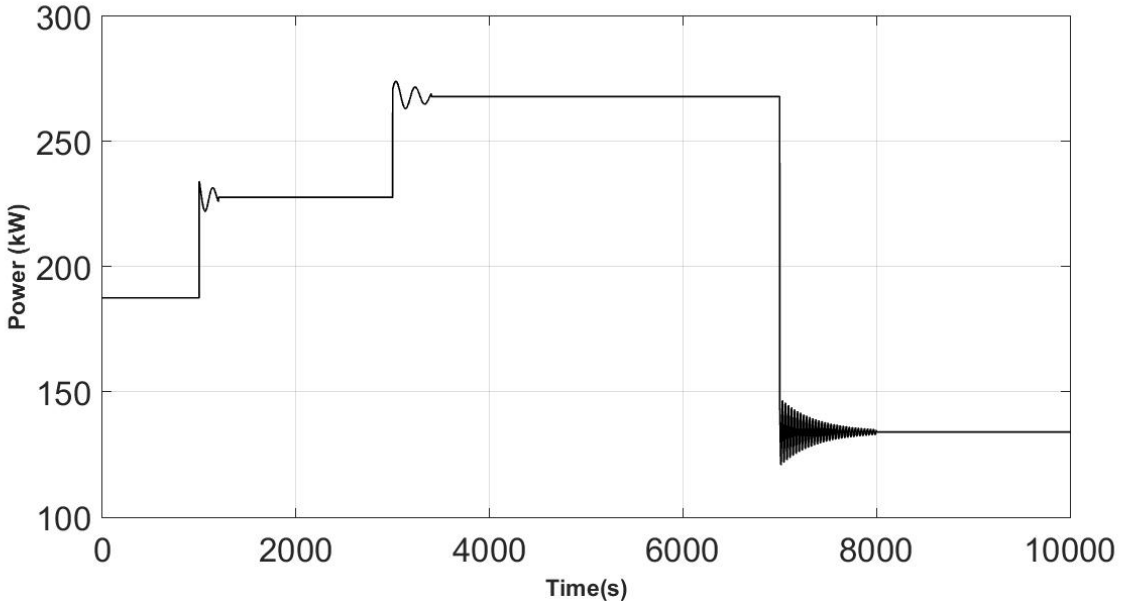

Figure 30. Power Demand Profile Applied to the Bloom Energy 268 kW SOFC System.

Figure 31 shows the response of the SOFC current to the power demand profile of the Bloom Energy system. A sensitivity analysis is conducted to investigate the effect of the steam to carbon (S/C) ratio on the SOFC current production. It could be observed that the SOFC produced more current as shown in the higher S/C ratio in Figure 31.

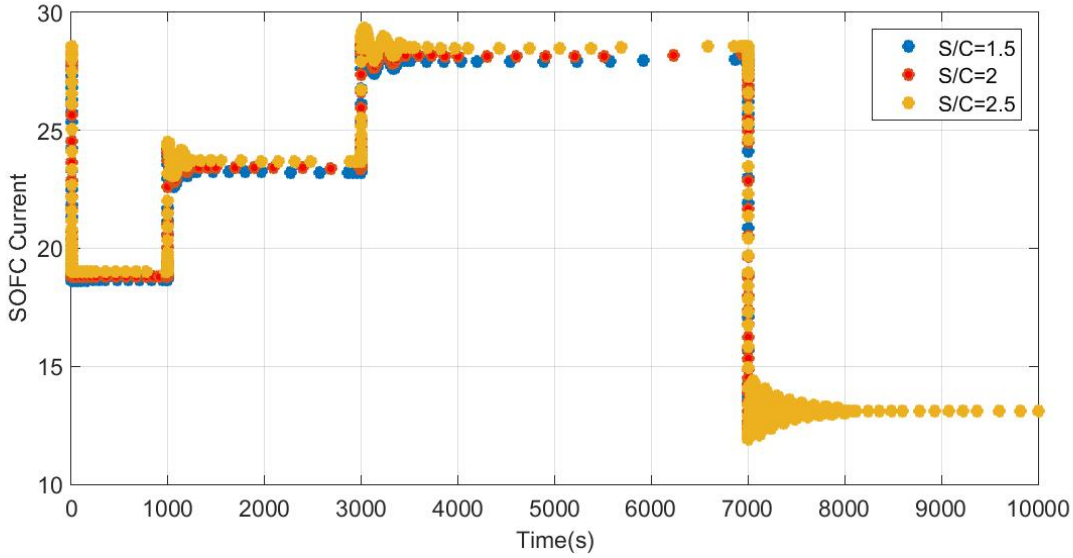

Figure 31. SOFC Current Variation for a 268 kW Bloom Energy SOFC.

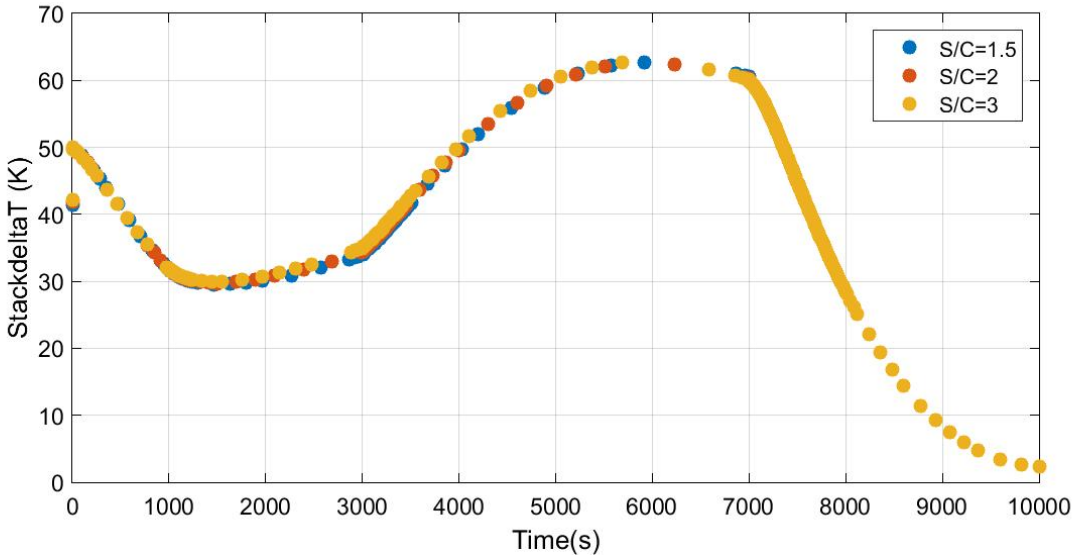

Figure 32. Stack Temperature Difference Variation for the Simulation of a 268 kW Bloom Energy SOFC.

As the power increases the stack temperature difference increases (see Figure 32), which is followed by decreasing stack temperature difference at t=7,000 s, as the power demand decreases.

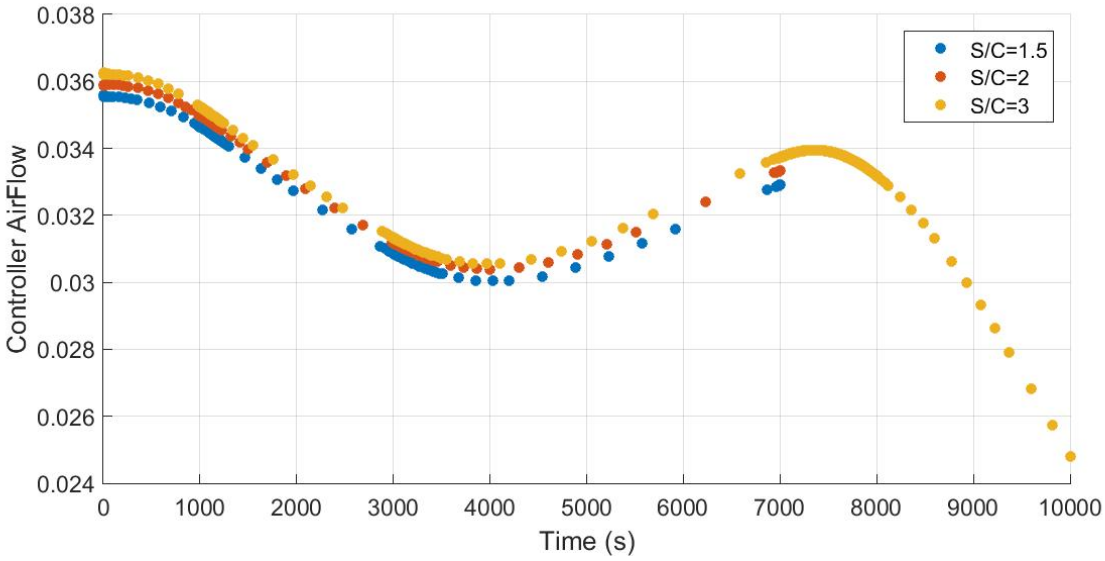

Figure 33. Controller Airflow Rate for the 268 kW Bloom Energy SOFC System.

Figure 34 shows that the oxygen utilization increases as the power demand increase and decreases with the power demand trend. Figure 35, Figure 36, Figure 37, and Figure 38 show the performance parameters of the 268 kW Bloom Energy system.

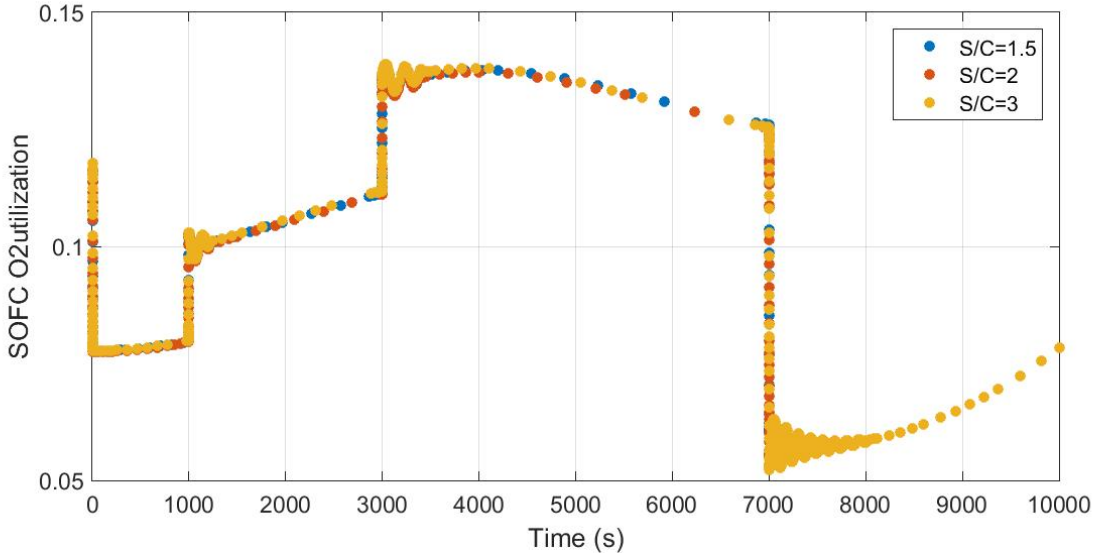

Figure 34. SOFC Oxygen Utilization for the 268 kW Bloom Energy System.

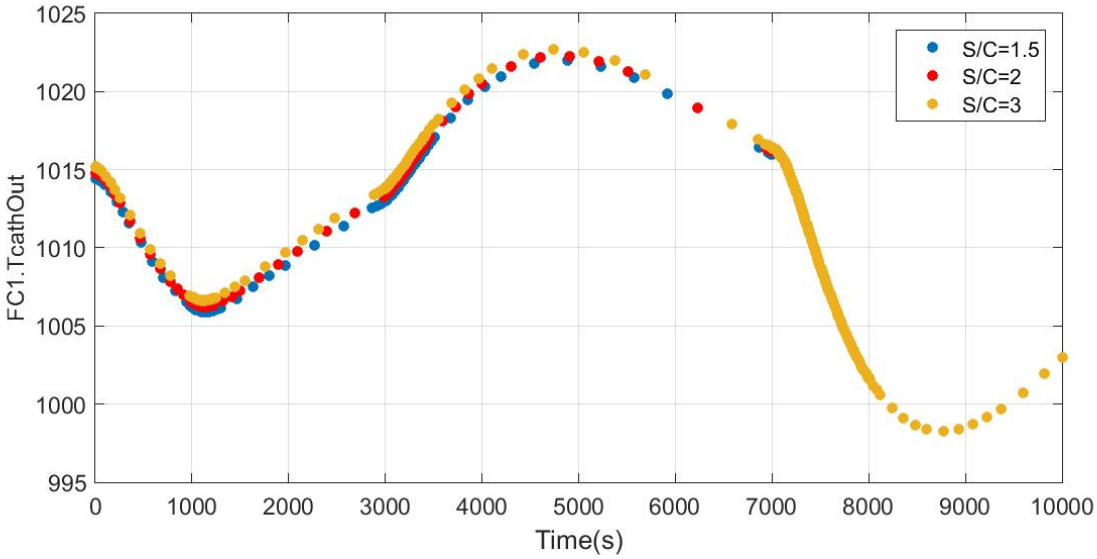

Figure 35. SOFC Cathode Outlet Temperature for the 268 kW Bloom Energy System.

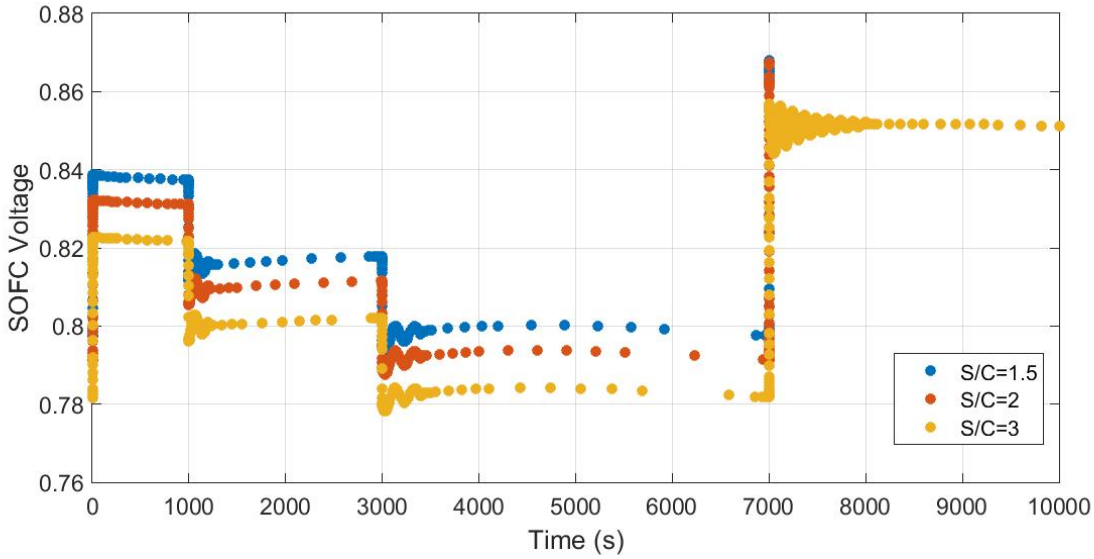

Figure 36. SOFC Voltage Variation for the 268 kW Bloom Energy System.

Note that the fuel cell tri-layer, comprised of a positive electrode, electrolyte, and negative electrode (PEN), is the main fuel cell component that is simulated. Note that the PEN temperature is resolved in two dimensions so that the PEN average temperature shown in Figure 37 is the spatial average versus time. Note that the PEN average temperature roughly increases when power demand increases and decreases as power demand decreases.

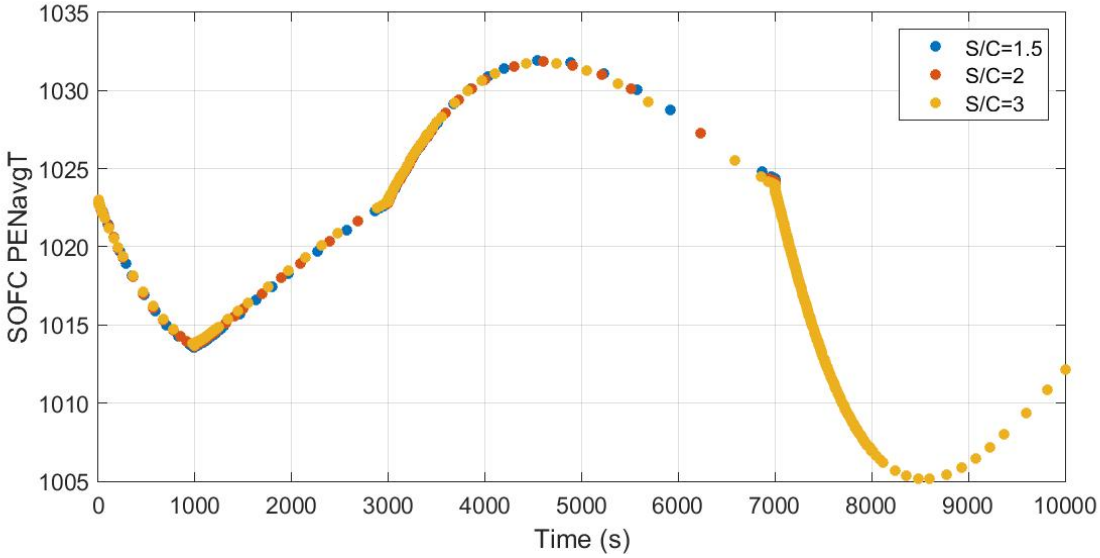

Figure 37. 268 kW Bloom Energy SOFC PEN Average Temperature.

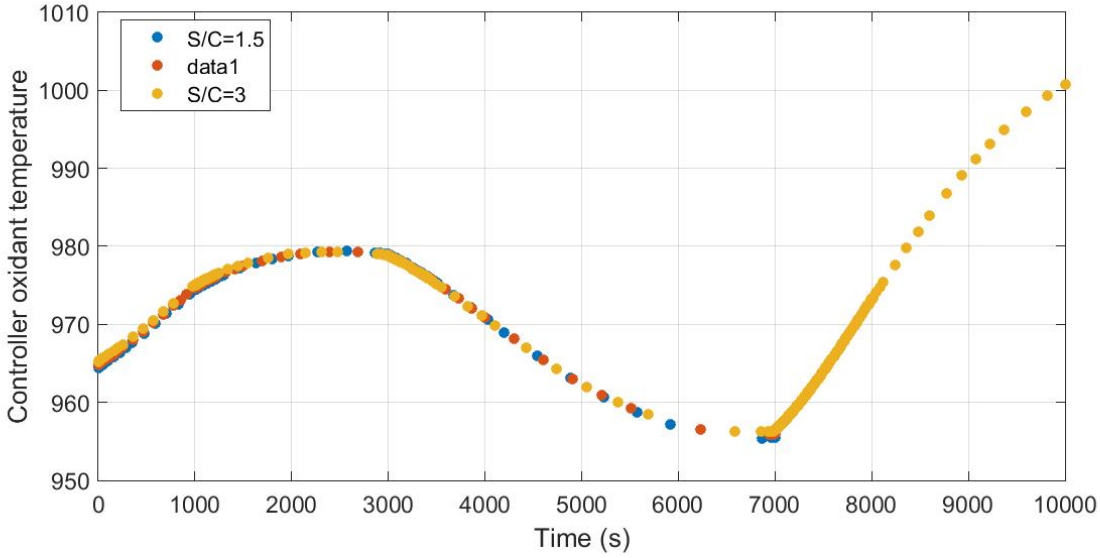

Figure 38. Controller Oxidant Temperature for the 268 kW Bloom Energy System.

Figure 39 shows the two-dimensional temperature profile over the PEN layer for the fuel and air flow configuration at the final point of operation t=10,000 s.

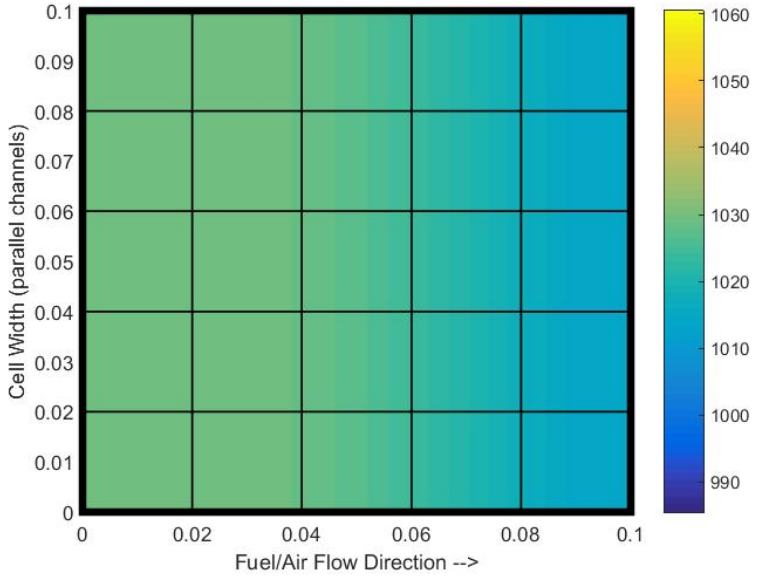

Figure 39. Temperature Profile of the 268 kW Bloom Energy System.

2.7 Results for 400 kW SOFC system of Versa Power

Versa Power (now owned by FuelCell Energy) has developed a solid oxide fuel cell system in the 400- kW size class that is comprised of a different cell and stack technology as well as a different system configuration. For example, the Versa Power cell design is anode-supported (i.e., the main structural component of the cell is the anode) while that of Bloom Energy is electrolyte-supported. A dynamic model of the Versa Power 400 kW system was developed and the same step-wise power demand that is similar to notched locomotive power demand requirements is applied. Figure 40 shows the

dynamics of the SOFC current that are experienced by the 400 kW Versa Power system under these operating conditions. Note the oscillations that occur near each step change in power demand, but otherwise steady current in between.

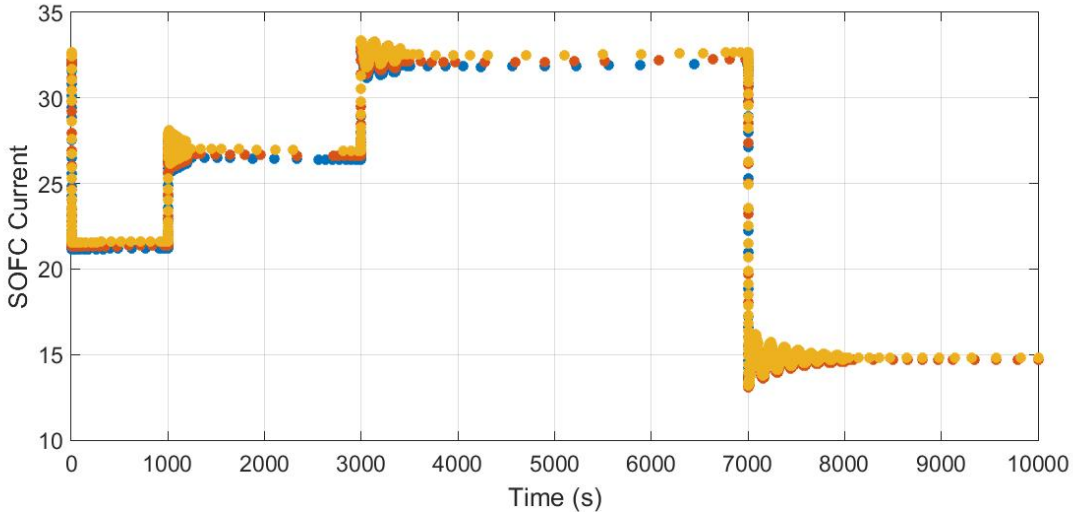

Figure 40. Current Dynamic Variation of the 400 kW Versa Power Type of SOFC.

Figure 41 shows the dynamics of oxygen utilization for the simulation of a 400 kW Versa Power type of SOFC system, which shows oxygen utilization generally increasing as power demand increases. Figure 42 shows the response of the 400 kW SOFC system cathode temperature to the power demand dynamics applied. Note that the thermal mass of the SOFC system delays and dampens the thermal response (compared to the electrochemical and flow responses), but, that generally cathode temperature increase as power demand increases, as expected.

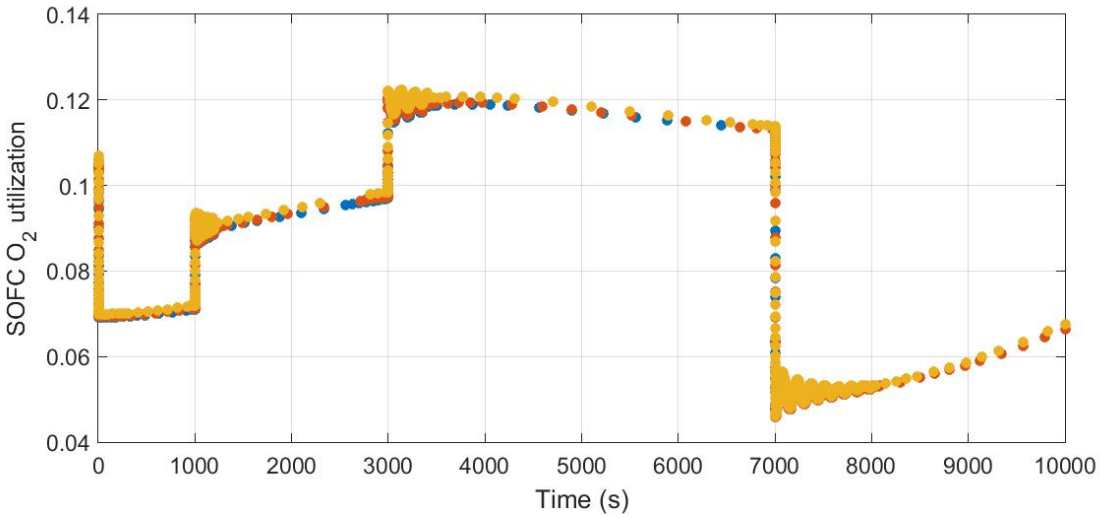

Figure 41. SOFC Oxygen Utilization of the 400 kW Versa Power Type of SOFC System.

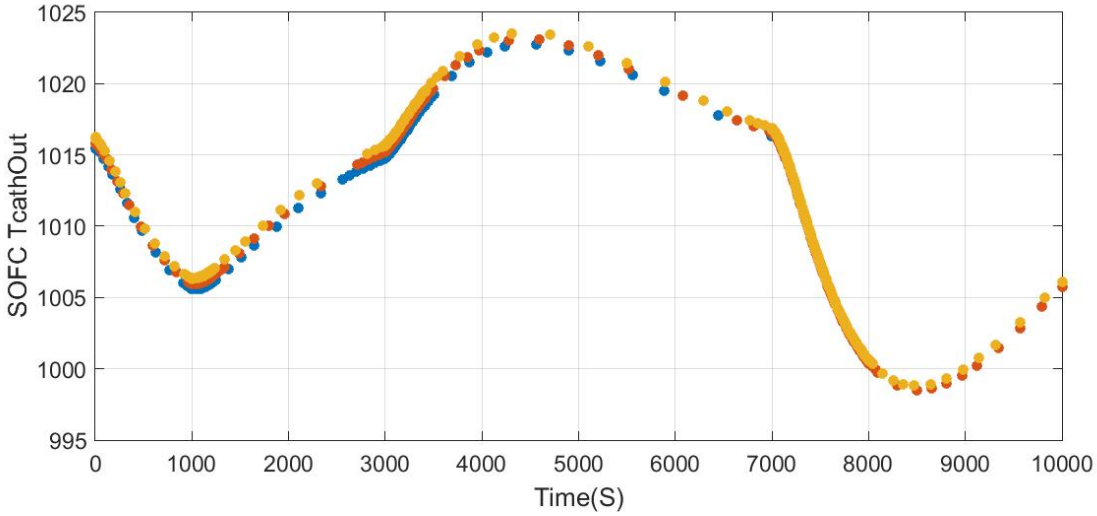

Figure 42. SOFC Cathode Temperature for the 400 kW Versa Power Type of System.

The voltage response of the Versa Power type of 400 kW SOFC system is shown in Figure 43 for three different operating steam-to-carbon ratios (S/C = 1.5, 2, and 3). Note that typically the voltage is higher for the lower S/C ratios. The controller oxidant temperature for the 400 kW Versa Power type of SOFC system as it responded to the applied power dynamics is shown in Figure 44. Note that temperature is gradually increased during times of lower power demand to maintain operating temperatures in a safe range.

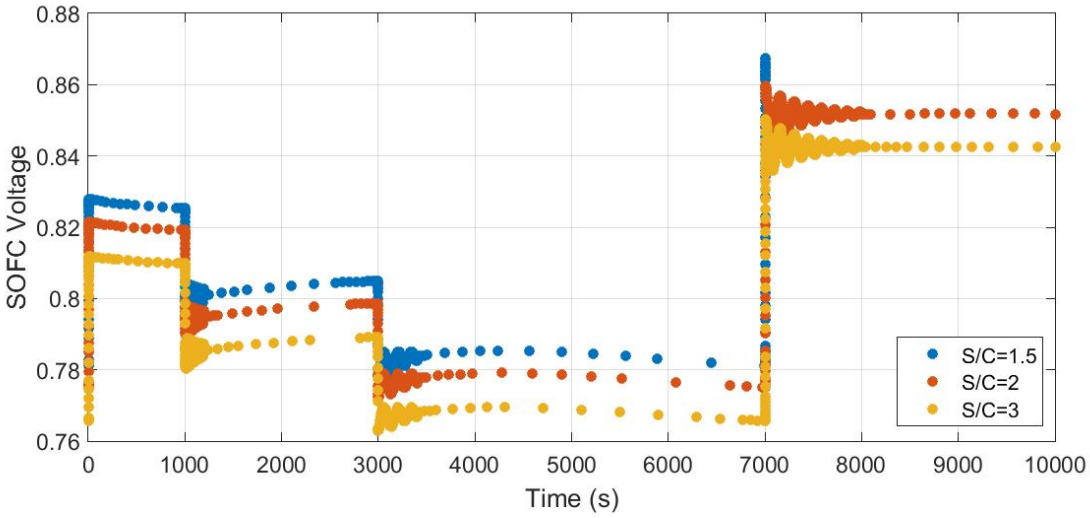

Figure 43. SOFC Voltage Changes for the 400 kW SOFC Versa Power Type of System for Three Different S/C Ratios.

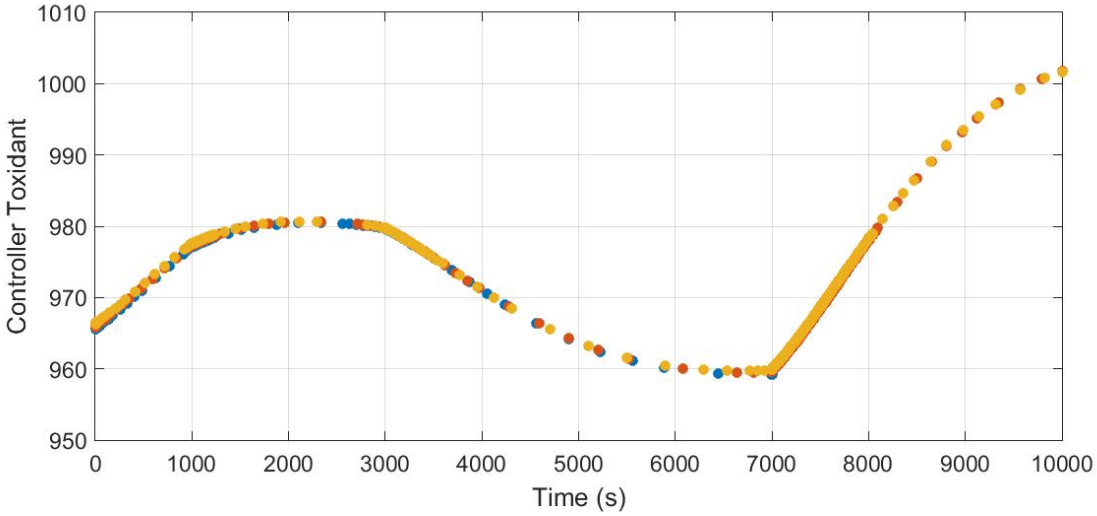

Figure 44. Controller Oxidant Temperature for the 400 kW Versa Power Type of SOFC System.

Figure 45 shows the controller air mass flow rate for the dynamic simulation of a 400 kW Versa Power type of SOFC system. When subjected to the step-wise transient power demand, the air flow rate

Figure 45 shows the controller air mass flow rate for the dynamic simulation of a 400 kW Versa Power type of SOFC system. When subjected to the step-wise transient power demand, the air flow rate controller manipulates air flow as shown in Figure 45.

The resulting PEN temperature distribution for the 400 kW Versa Power SOFC dynamic simulation is presented in Figure 46. Note the relatively uniform temperature that is achieved for this condition at the very end of the dynamic simulation (t = 10,000 s) during which time the power demand is fairly low (125 kW).

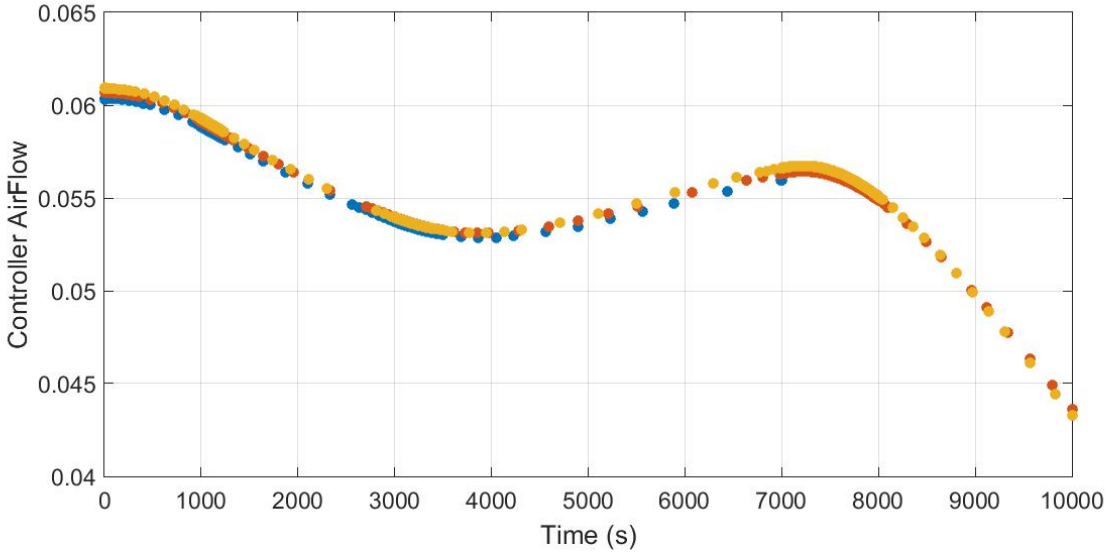

Figure 45. Controller Air Mass Flow Rate for the Simulation of a 400 kW Versa Power SOFC System.

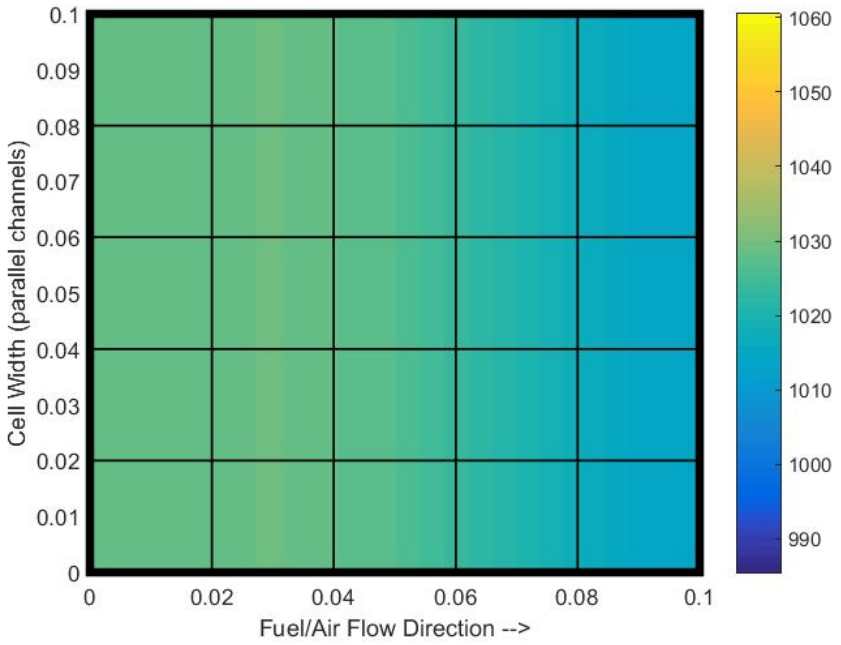

Figure 46. Temperature Profile for the 400 kW Versa Power SOFC System at the End of All Transient Responses (t = 10,000 s).

2.8 Capstone C-200 Turbo-Machinery Dynamic Response

The performance of the turbo-machinery of the hybrid SOFC-GT system when subjected to the same step-wise power demand (similar to notched locomotive power demand requirements) is presented in this section. Figure 47 presents the dynamic efficiency response of the Capstone C-200 micro turbine when subjected to the notched power demand dynamics. Note that the efficiency is typically in the range of 15 to 23 percent during the entire period of the simulation, which is in the range of expectations for turbomachinery that when fired directly by combustion of natural gas has an efficiency of around 33 percent. Note that when operating in a hybrid system, the turbine is fired only with the "waste heat" of the SOFC and, as a result of this much lower quality (lower temperature) heat, experiences a de-rate of efficiency of between 30 and 54 percent.

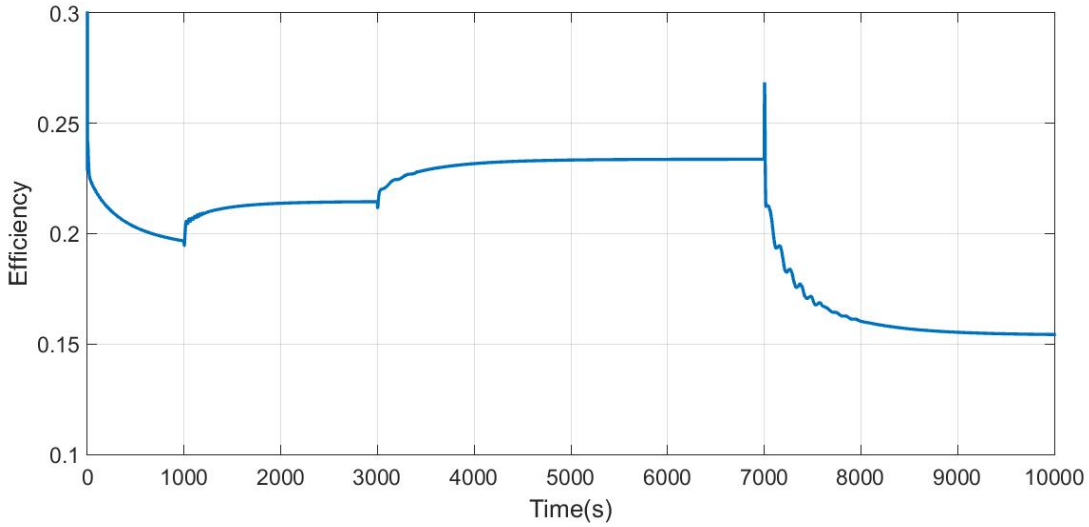

Figure 47. Efficiency Dynamics of the Capstone C-200 Micro Turbine Over t=10,000 s in Response to the Notched Power Demand Dynamics.

Figure 48 shows that stack temperature difference for the entire simulation. Note that this stack temperature difference is that which drives the Capstone turbo-machinery to produce power and air flow to the stack.

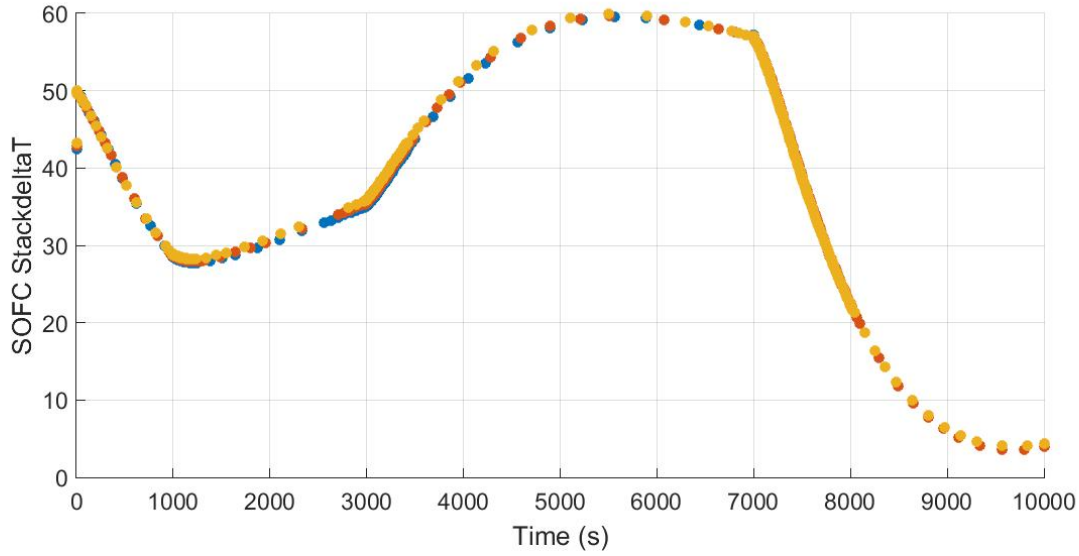

Figure 48. Stack Temperature Difference Variation Over t=10,000 s.

The dynamic variations in RPM experienced by the Capstone C-200 engine during the simulation are presented in Figure 49. Note that the controller is always attempting to keep turbine speed at about 61,000 RPM. The control is quite good, but, most significantly departs from this set point during the sharp power demand decrease that occurs at around 7,000 s.

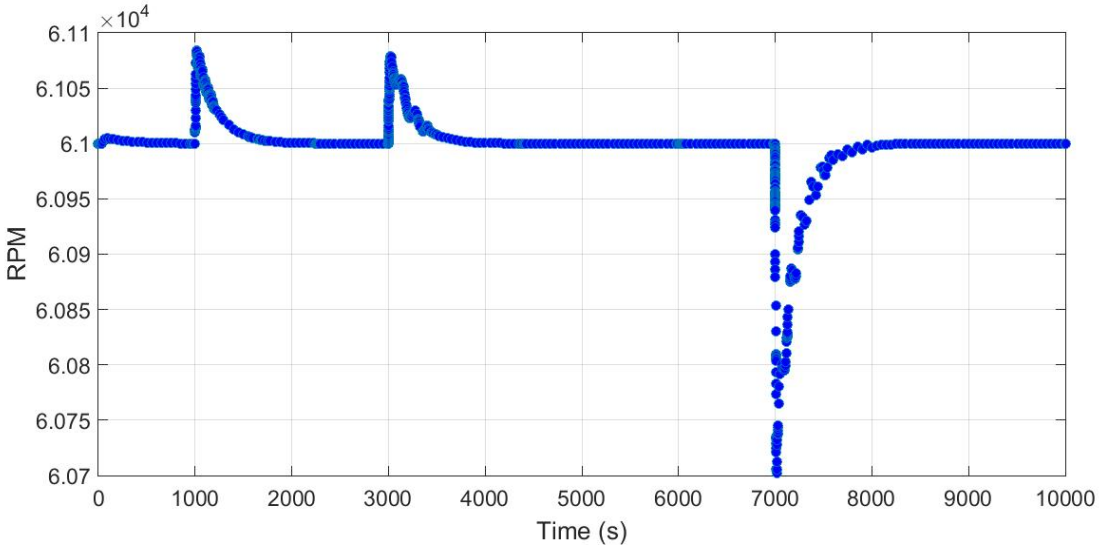

Figure 49. RPM Variation in C-200 Capstone Micro Turbine Transient Operation.

3. System Sizing

Figure 50 shows the SOFC stack and bundle sizing schematic and how the size is calculated.

Figure 50. SOFC Stack Sizing.

Figure 51 and Figure 52 show the sizing of the fuel preheater and air recuperator heat exchangers, which are the main two heat exchangers used in the hybrid SOFC-GT system.

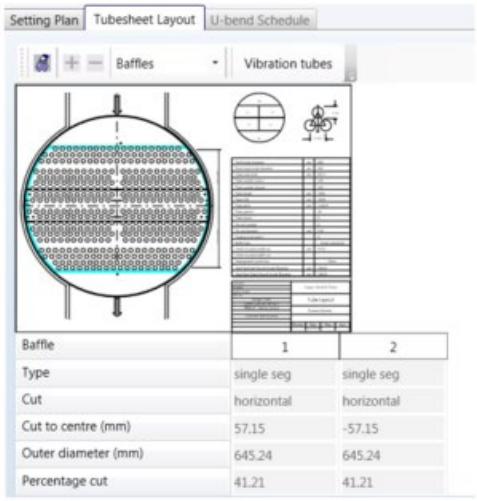

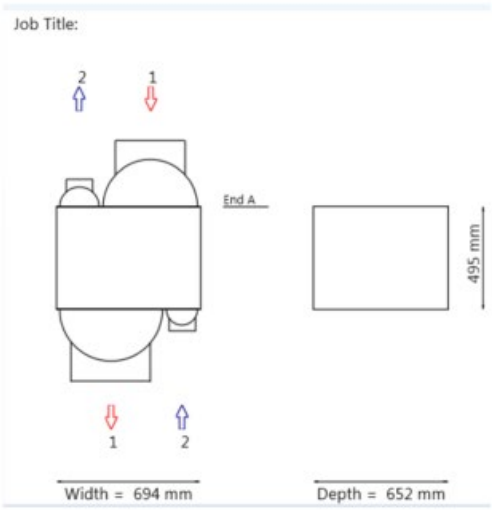

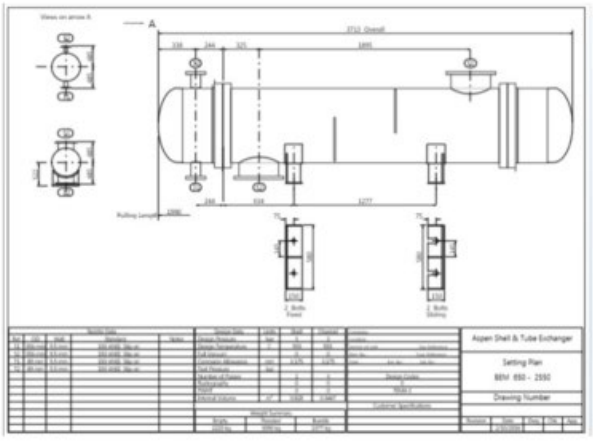

Figure 51. Fuel Preheater Sizing.

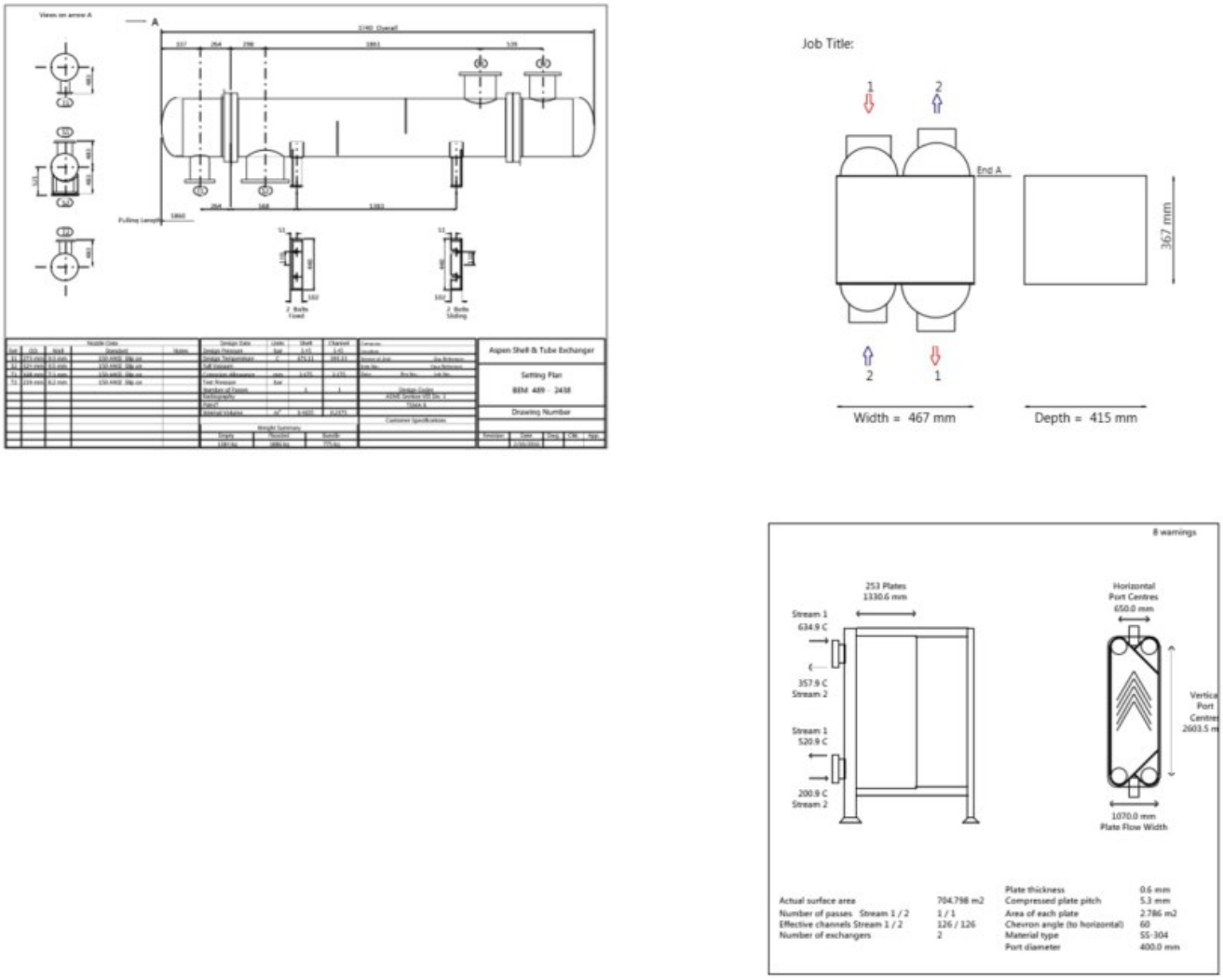

Figure 52. Air Recuperator Sizing.

Figure 53, Figure 54, and Figure 55 shows the schematic of the main engine. The plan consists of the Kawasaki GT, 3 MW SOFC stacks, diesel reformers, two heat exchangers, a fuel tank, and the associated piping and valves. The plant size is compared to the current locomotive size.

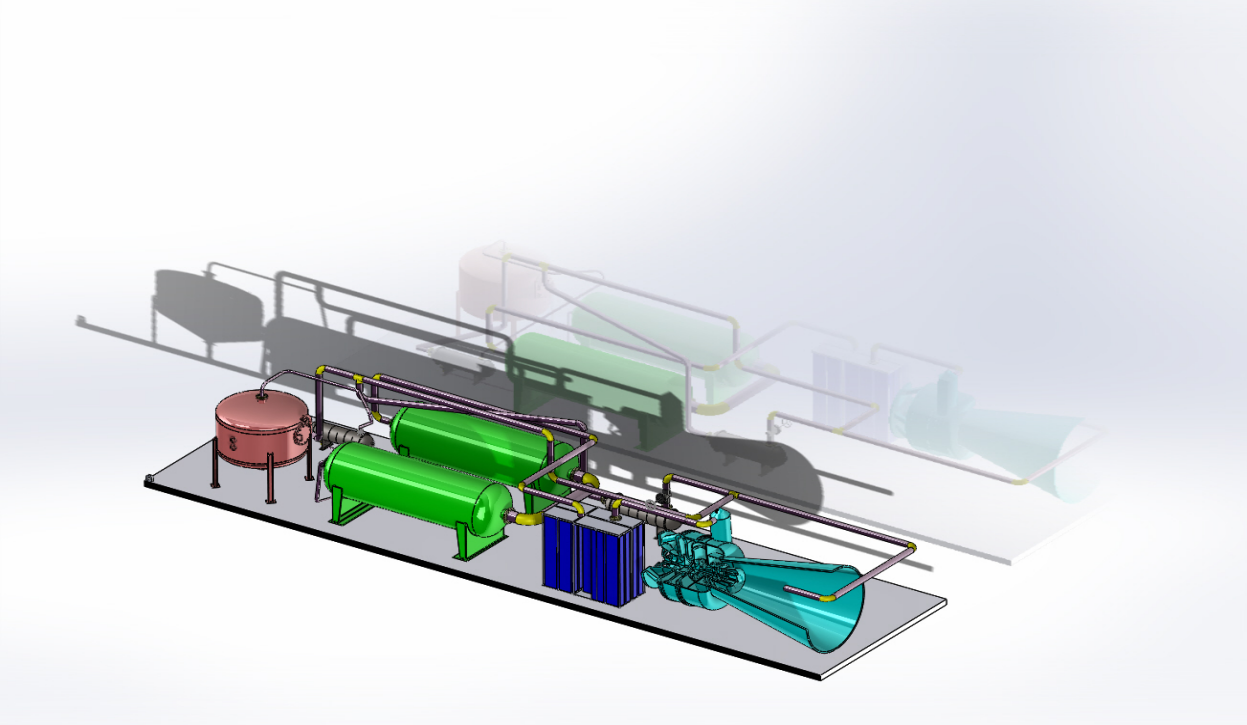

Figure 53. Hybrid SOFC-GT Plant Sizing.

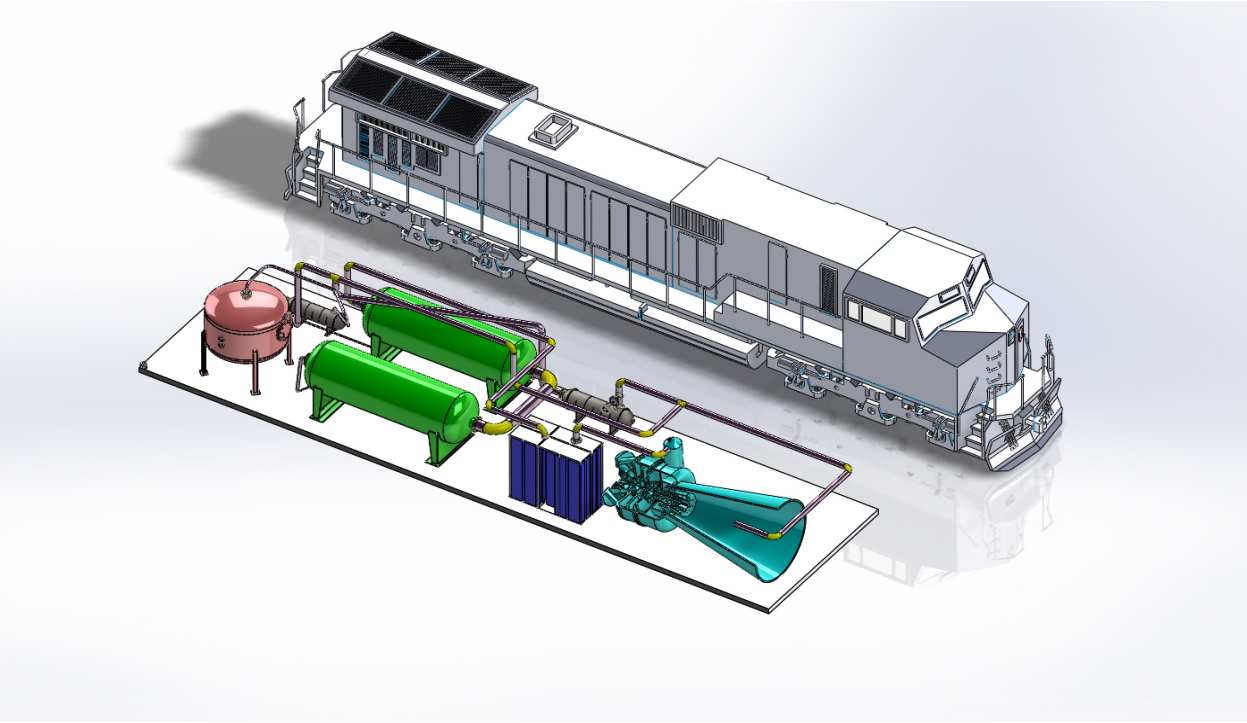

Figure 54. 4 MW SOFC-GT System Size Compared to the Actual Size of the Locomotive.

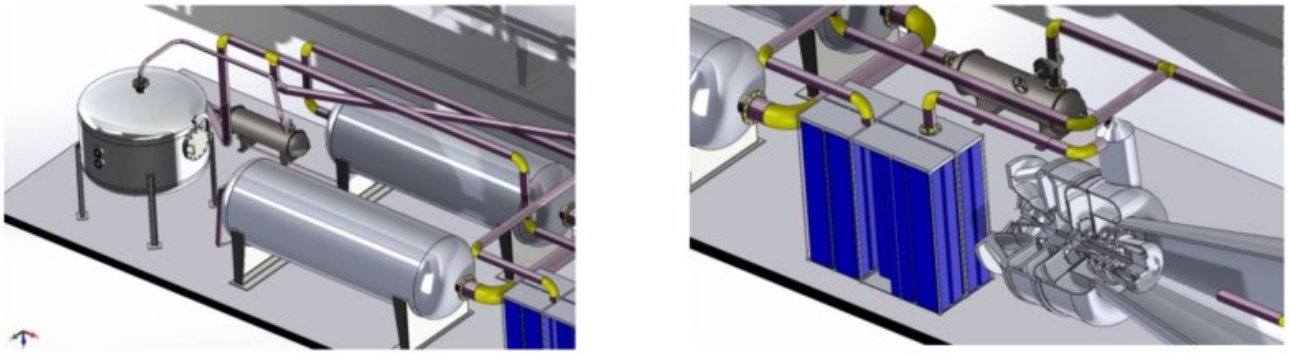

Figure 55. Modification of the Main Components of the System (Gas Turbine).

4. Fuel Cell – Reciprocating Engine Hybrid Locomotive

A steady-state system analysis of a 4 MW solid oxide fuel cell-reciprocating engine (SOFC-RE) hybrid system for a locomotive application has also been analyzed. The initial results included the determination of a combined hybrid efficiency of 53.4 percent for a range of fuel utilizations from 80 percent to 85 percent. This efficiency was disappointingly low, so that, additional analyses of this type of hybrid system were accomplished with some significant changes to the model and the analyses to accurately reflect the performance of the newest state-of-the-art fuel cell systems and reciprocating engines. The results that were achieved for these changes are presented in this section followed by a design of a smaller prototype hybrid system as is required for initial testing the hybrid concept on a railway test bed.

4.1 Updated Results

Previously, the SOFC stack and SOFC-RE hybrid efficiency was investigated as a function of fuel utilization. To obtain a higher efficiency compared to that of real-life SOFC systems, some changes to the model were made. The new voltage-current(V-I) curve, and efficiency plots achieved with the updated model parameters for the SOFC-RE system are displayed below in Figure 56 and Figure 57, respectively. The voltages that the fuel cells are able to achieve in the updated simulation are in the range of 0.80 to 0.84, (Figure 56) which were achieved by simulated reductions in activation and ohmic losses. As a result, the SOFC efficiency (Figure 57) that can be achieved is in the range of 63 to 68 percent.

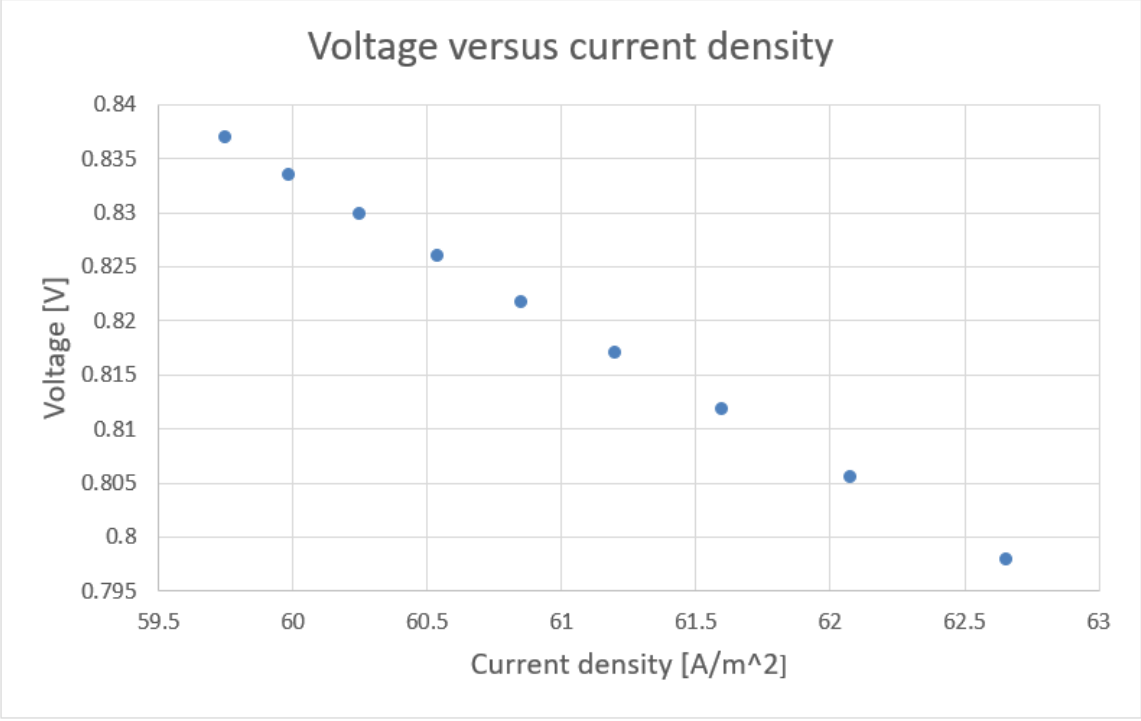

Figure 56. Polarization Curve for SOFC Used in SOFC-RE System Design.

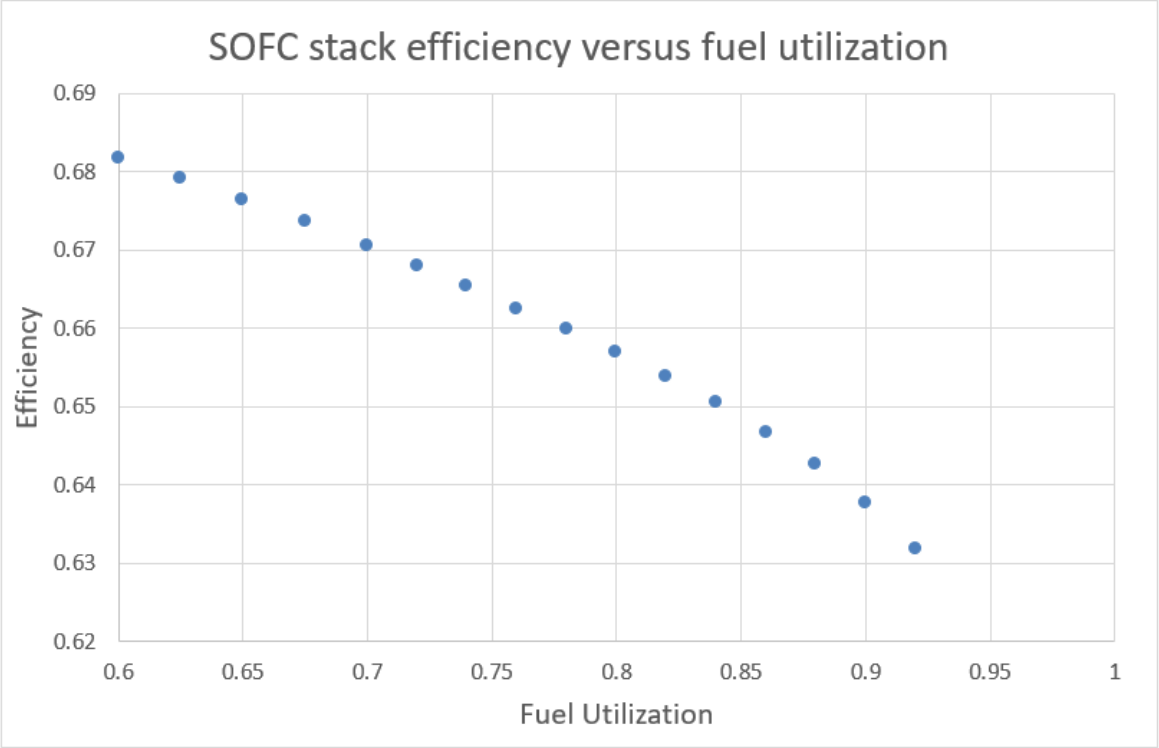

Figure 57. Effect of Fuel Utilization upon Stack Efficiency for the SOFC Used in SOFC-RE System Design.

From Figure 56 it is evident that the SOFC is now operating at a higher voltage and lower current density due to the reduced losses. The voltage drop with increasing current density is essentially linear, meaning that for the range of fuel utilizations studied, the fuel cell is operating in the region where ohmic polarization dominates.

Figure 57 shows that the fuel cell model has been improved to obtain a stack efficiency of around 63 percent and higher as the utilization is kept under 95 percent. This fuel cell performance was then investigated by integrating the SOFC with a reciprocating engine (RE). The reciprocating engine selected is the Caterpillar model CAT® CG132-16 800 kWe gas generator with a maximum efficiency of 42.8 percent when fired with combustion of relatively low energy content gas. This engine is the new RE of choice because it can convert gas mixtures with a relatively low energy density directly into electricity, which simplifies the system design.

Using the updated fuel cell stack performance and gas generator, the hybrid system efficiency has been recalculated and plotted for the steady state case as shown in Figure 58.

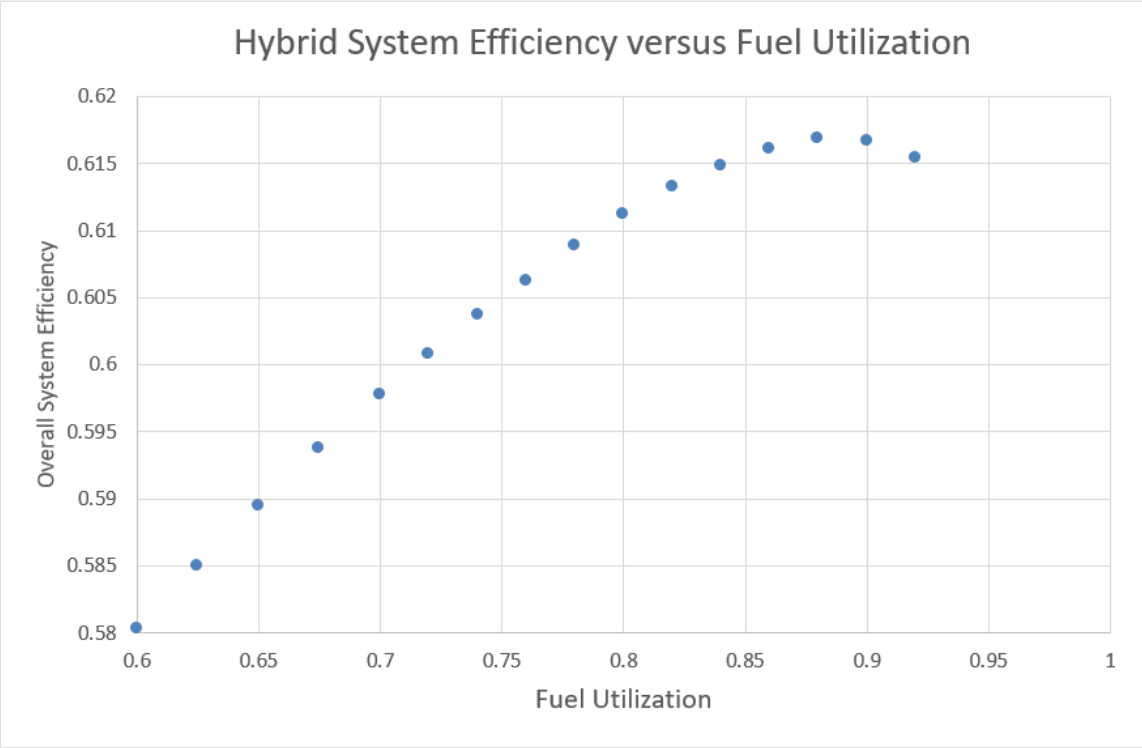

Figure 58. Hybrid SOFC-RE System Efficiency.

Due to the increased difference between SOFC and RE efficiency, the hybrid system efficiency now peaks at a higher fuel utilization. The maximum hybrid efficiency is 61.7 percent at a utilization of 88±2percent.

4.2 300 kW Prototype Design

Due to the necessity of testing a smaller prototype hybrid system before building the first long-haul locomotive engine, a hybrid system design which fits onto a locomotive test platform must be devised. Currently, the best available SOFC system is the Bloom Energy ES-5710 Energy Server with 250 kW AC output power and a size of 26’5’’x8’7’’x6’9’’ (8.06 m x2.62 m x2.06 m).

A suitable RE to convert the leftover fuel from this SOFC is the Kohler 60REZGB gas generator with a prime rating of 53 kW and an efficiency of 31.7 percent. This efficiency was calculated from the application data in the specification sheet found on the Kohler® website. The researchers are enquiring about the possibility of operating this generator on syngas from the anode off-gas rather than natural gas. The updated system diagram is displayed in Figure 59. The system was designed by Dustin Mclarty of UCI and Masoud Rokni of Technical University of Denmark - Copenhagen; and modeled by Allen Schellerup of UCI.

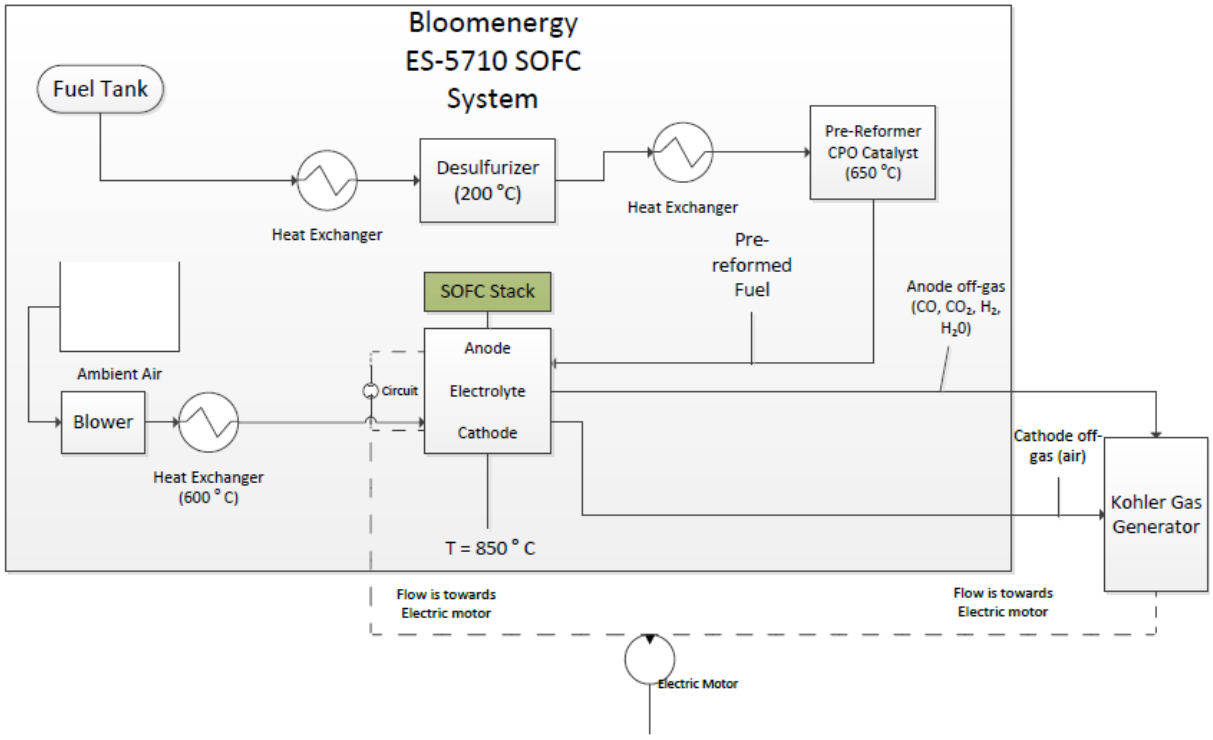

Figure 59. SOFC-RE System Design.

This diagram shows that there are three main system components: the SOFC, the gas generator, and the electric motor. The fuel is desulfurized, pre-heated and pre-reformed (catalytic partial oxidation to syngas) before entering the SOFC stack at 650 °C. Ambient air is blown through a heat exchanger where it is pre-heated to 600 °C before it enters the stack. Inside the SOFC stack, internal reforming converts methane to syngas at 780 °C. Since the fuel utilization must be less than 100 percent, the SOFC does not convert all fuel to electricity. Hence, the anode off-gas contains a syngas-air mix which is directed into the gas generator (or, more generally, the RE). Simultaneously, the cathode off-gas (air) is sent directly into RE where it is compressed. Expansion work drives the generator inside the RE to generate additional electricity, improving the overall system efficiency. Finally, the electricity from both the SOFC and RE is used to power the locomotive's electric motor that is connected by a circuit.

Depending on the results of the enquiry with Kohler®, the need for steam removal along the anode off-gas stream to increase the energy density of the RE input fuel may arise. The following drawing visualizes the dimensions of fitting the prototype system onto a standard locomotive.

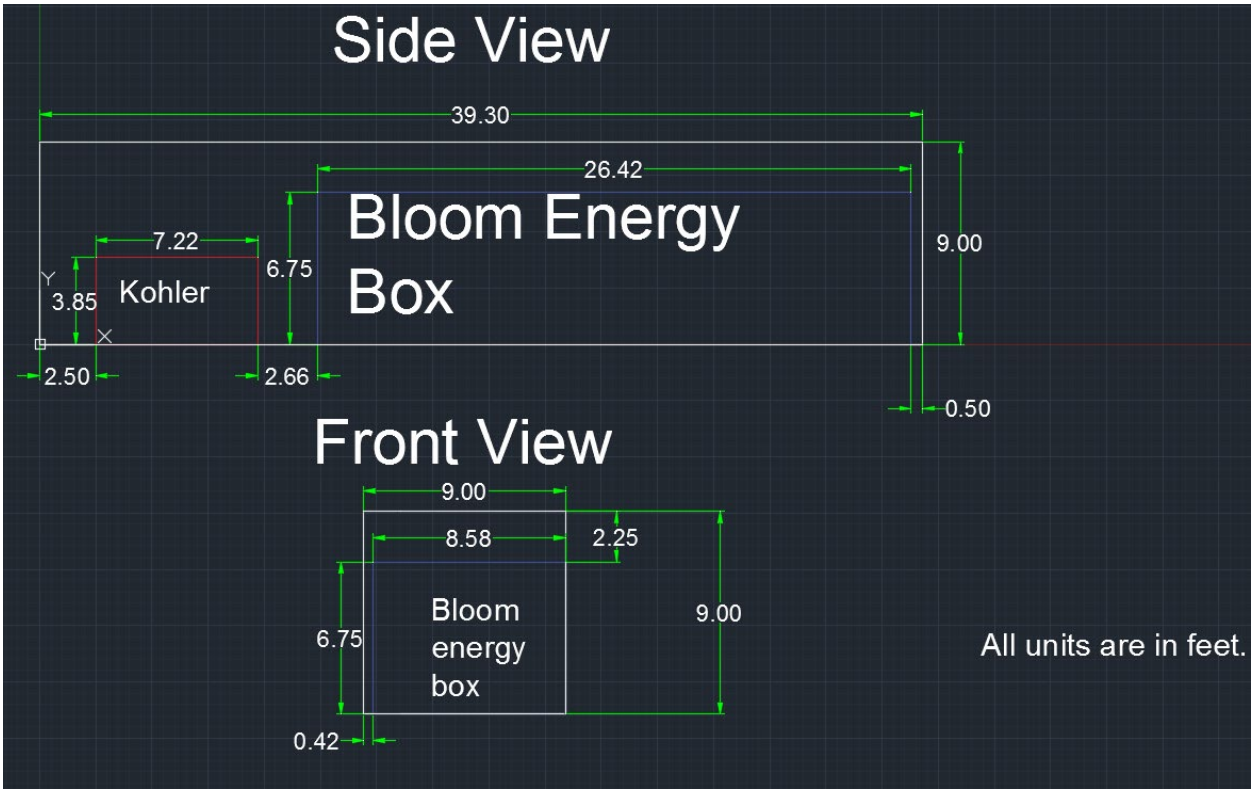

Figure 60. Sizing of the SOFC-RE Prototype System Design in Comparison To Engine Compartment of a Locomotive.

The white rectangles show the available space inside an MLW M-636 2700 kW locomotive—39.30 feet long, 9.00 feet wide, and 9.00 feet high. The dimension with the tightest fit is the width where only 1.5 feet of walking space were allowed on one side of the Bloom Energy server (the SOFC). Regarding the length, the SOFC sits mainly in the space that is usually empty on a locomotive, while the gas generator is placed into what is normally the engine compartment. Sufficient space for piping and heat exchangers was allowed between and above the two components.

It was calculated that for the RE to operate at its prime rating using the anode off-gas, the fuel utilization of the SOFC must be reduced to about 76 percent. This also reduces the prototype hybrid efficiency to 57.9 percent. Note that this efficiency is lower than the 4 MW system because smaller REs are less efficient, but it is still acceptable for the purpose of testing a prototype. The full desired operating parameters of this prototype hybrid are tabulated below.

Table 5. Steady State Performance Characteristics Expected from the SOFC-RE System Comprised of a Single Bloom Energy 5710 Server Integrated with a Kohler 60 REZGB Gas Generator.

Fuel Utilization	0.76
Operating Voltage	0.8369 V
Power from SOFC	250 kW
Fuel Cell Efficiency	0.5035
RE Efficiency	0.317
RE Output	53 kW
Total System Output	303 kW
Total system Efficiency	0.579
Flow Rate into SOFC	2.657 mol/s
Flow Rate anode off-gas	2.768 mol/s

Note that the molar flow rate out of the SOFC anode is slightly higher than the SOFC inlet flow rate, but the mass flow rate out of the anode is more than twice the inlet flow rate because of the oxygen bound in the water adding to the molar mass of the anode off-gas. This high flow rate of stream containing a 70 percent mole fraction of stream might be avoided by placing a condenser along the anode off-gas stream, which will only allow the syngas mixture to pass through into the RE.

4.3 Components Used in the Prototype SOFC-RE System Design

Images of the components used in the Prototype SOFC-RE systems analyzed in this work are shown in Figure 61, Figure 62, and Figure 63. The Caterpillar model CAT® CG132-16 gas generator is shown in Figure 61, while the Kohler model 60REZGB gas generator is shown in Figure 62. An image of the Bloom Energy® ES-5710 SOFC system is presented in Figure 63.

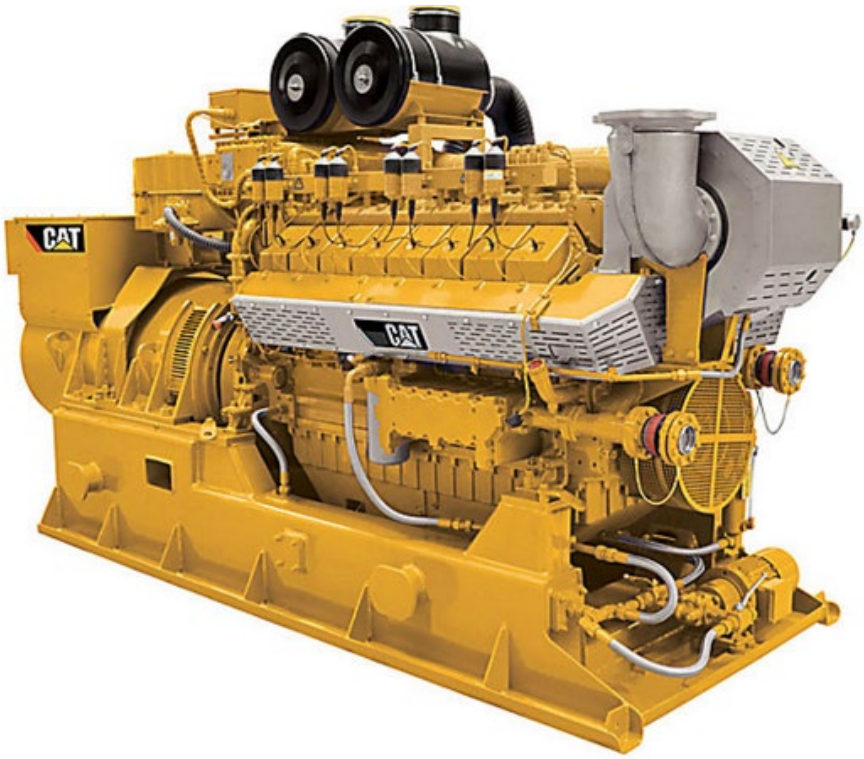

Figure 61. CAT® CG132-16 Gas Generator.

Figure 62. Kohler 60 REZGB Gas Generator.

Figure 63. Bloom Energy ES-5710 Solid Oxide Fuel Cell System.

5. Conclusion

In this research, challenges related to the use of hybrid SOFC-GT technology in a locomotive application were investigated. The challenges include compressor stall/surge and step-wise notching power demand dynamics of a typical locomotive that may significantly affect hybrid SOFC-GT system performance. The researchers at NFCRC designed a single-stage compressor, similar to the compressor used in a 200 kW Capstone Turbines micro gas turbine. This compressor could be used in a 500 kW hybrid SOFC-GT locomotive test engine, that could eventually be tested at the NFCRC. The transient operation of this industrial centrifugal compressor performance using CFD tools was analyzed, which provided insights regarding the flow distribution in the compressor impellers. To simulate the real world compressor operation in the 500 kW test hybrid SOFC-GT system, a transient pressure boundary condition that resulted from a hybrid system dynamic simulation was applied to the compressor configurations. The pressure step change that resulted from the transient hybrid system response to a load perturbation, corresponds to a sudden change of compressor dynamics near the surge limit line. The single-stage compressor was shown to be robust to the pressure dynamics and as a result is deemed suitable for use in hybrid SOFC-GT systems for locomotive applications. The single-stage compressor was able to keep air flow over the period of transient operation that prevents the flow entering the severe deep surge region, which could lead to hybrid system failure.

A MATLAB SOFC-GT simulation platform was developed for components of the hybrid SOFC-GT system that could capture the transient operation of a hybrid engine in a locomotive as a response to the locomotive power requirements. Initial results of the fuel cell and GT are obtained, presented and discussed. The feasibility of the hybrid SOFC-GT system is investigated regarding system sizing for a future SOFC-GT system as applied to a full-scale long haul locomotive and a current SOFC-GT system for application to a locomotive test platform BOP and the main components of the system are sized through detailed calculations and a general schematic of the system sizing that was provided by equipment manufacturers and compared to the actual size of the locomotive (GE dash 9). It was found that the sizing of the system was one of the challenges, however, it could be improved by developing better control algorithms that will reduce the BOP sizing and the main component sizes. Also, the system could be manufactured in a more compact form, especially as SOFC current densities are expected to improve over time, which will allow the SOFC-GT system to fit into the locomotive engine platform.

6. References

1. Barelli, L., Bidini, G., and Ottaviano, A. (2012). Part load operation of SOFC-GT hybrid systems: Stationary analysis. *International Journal of Hydrogen Energy*, *37*(21), p. 16140–16150.
2. Brouwer, J. Hybrid gas turbine fuel cell systems.
3. Dincer, I., and Colpan, C. O. (2013). Introduction to Stationary Fuel Cells, Ni, M., and Zhao, T. S. *Solid Oxide Fuel Cells: From Materials to System Modeling.* The Royal Society of Chemistry, p. 1–25.
4. Ferrari, M.L., Pascenti, M., Bertone, R., and Magistri, L. (2009). Hybrid Simulation Facility Based on Commercial 100 kWe Micro Gas Turbine. *Journal of Fuel Cell Science and Technology*, *6*(3):031008.
5. Ferrari, M. L., Pascenti, M., Magistri, L., and Massardo, A. F. (2010). Hybrid System Test Rig: Start-up and Shutdown Physical Emulation. *Journal of Fuel Cell Science and Technology*, *7*(2):021005.
6. U.S. Department of Energy. (April 2002). Fuel cells for Buildings and Stationary Applications Roadmap. Workshop Proceedings.
7. Capstone Turbine website.
8. Obermeyer, F. (2014). Practical application and experience with micro gas turbines. 56th Würzburg Brick and Tile Training Course 2017.
9. Kawasaki gas turbines-americas gas turbines power generation technology & applications.
10. Kaswasaki gas turbine generator sets, Kawasaki heavy industries.
11. Lindermeir, A., et al. (2007). "On-board diesel fuel processing for an SOFC–APU—Technical challenges for catalysis and reactor design." *Applied Catalysis B: Environmental, 70*(1–4), p. 488–497.
12. Martinez, A. S., Brouwer, J., and Samuelsen, G. S. (2012). Feasibility study for SOFC-GT hybrid locomotive power: Part I. Development of a dynamic 3.5 MW SOFC-GT FORTRAN model. *Journal of Power Sources*, 213, p. 203–217.
13. Martinez, A. S., Brouwer, J., and Samuelsen, G. S. (2012). Feasibility study for SOFC-GT hybrid locomotive power: part ii. System packaging and operating route simulation. *Journal of Power Sources*, 213, p. 358–374.
14. McLarty, D., Kuniba, Y., Brouwer, J., and Samuelsen, S. (2012). Experimental and theoretical evidence for control requirements in solid oxide fuel cell gas turbine hybrid systems. *Journal of Power Sources*, *209*, p.195–203.
15. McLarty, D., Brouwer, J., and Samuelsen, S. (2014). Fuel cell–gas turbine hybrid system design part I: Steady state performance. *Journal of Power Sources*, *257*, p. 412–420.
16. McLarty, D., Brouwer, J., and Samuelsen, S. (2014). Fuel cell–gas turbine hybrid system design part II: dynamics and control. *Journal of Power Sources*, *254*, p. 126–136.

17. McLarty, D. F. (2013). *Thermodynamic Modeling and Dispatch of Distributed Energy Technologies including Fuel Cell--Gas Turbine Hybrids*. PhD dissertation.

18. McPhee, W., Bateman, L., Koslowske, M., Slaney, M., Uzep, Z., Bentley, J., and Tao, T. (2011). Direct JP-8 Conversion Using a Liquid Tin Anode Solid Oxide Fuel Cell (LTA-SOFC) for Military Applications. *Journal of Fuel Cell Science and Technology*, *8*(4):041007.

19. O'Hayre, R. P., Cha, S., Colella, W., and Prinz, F. B. (2006). *Fuel cell fundamentals, Third Edition*. John Wiley & Sons New York.

20. Rajashekara, K. (2005). Hybrid fuel-cell strategies for clean power generation. *Industry Applications, IEEE Transactions on*, *41*(3), p. 682–689.

21. Rao, A. D., Samuelsen, G. S., Robson, F. L., and Geisbrecht, R. A. (2002). Power Plant System Configurations for the 21st Century. In: *ASME Turbo Expo 2002: Power for Land, Sea, and Air*, p. 831–844. American Society of Mechanical Engineers.

22. Samuelsen, S., and Brouwer, J. (2009). Fuel cell/gas turbine hybrid. *Encyclopedia of Electrochemical Power Sources*, p.124–134.

23. Sasaki, K., Watanabe, K., Shiosaki, K., Susuki, K., and Teraoka, Y. (2004). Multi-Fuel Capability of Solid Oxide Fuel Cells. *Journal of Electroceramics*, *13*(1–3), p. 669–675.

24. Singhal, S. C. (2002). Solid oxide fuel cells for stationary, mobile, and military applications. *Solid State Ionics*, 152, p. 405–410.

25. Staniforth, J., and Kendall, K. (2000). Cannock landfill gas powering a small tubular solid oxide fuel cell—a case study. *Journal of Power Sources*, *86*(1), p. 401–403.

26. Stiller, C., Thorud, B., Bolland, O., Kandepu, R., and Imsland, L. (2006). Control strategy for a solid oxide fuel cell and gas turbine hybrid system. *Journal of Power Sources*, *158*(1). p. 303–315.

27. Winkler, W., Nehter, P., Williams, M. C., Tucker, D., and Gemmen, R. (2006). General fuel cell hybrid synergies and hybrid system testing status. *Journal of Power Sources*, *159*(1), p. 656–666.

28. Zhang, X., Chan, S. H., Li, G., Ho, H. K., Li, J., and Feng, Z. (2010). A review of integration strategies for solid oxide fuel cells. *Journal of Power Sources*, *195*(3), p. 685–702.

Abbreviations and Acronyms

Abbreviations & Acronyms	Name
BOP	Balance of Plant
CFD	Computational Fluid Dynamics
I	Current
FC-GT	Fuel Cell Gas Turbine
GT	Gas Turbine
H_2	Hydrogen
kg	Kilogram
kW	Kilowatt
MW	Megawatt
MTG	Micro-Gas Turbine Generator
mol	Mole
NETL	National Energy Technology Laboratory
NFCRC	National Fuel Cell Research Center
lbm	Pound Mass
PEN	Positive Electrode, Electrolyte, and Negative Electrode
C_3H_8	Propane
RE	Reciprocating Engine
RPM	Revolutions Per Minute
RANS	Reynolds Averaged Navier-Stokes
s	Second
SST	Shear Stress Transport
SOFC	Solid Oxide Fuel Cell
SOFC-GT	Solid Oxide Fuel Cell-Gas Turbine
SOFC-RE	Solid Oxide Fuel Cell-Reciprocating Engine
S/C	Steam to Carbon
t	Time
TIT	Turbine Inlet Temperature
UCI	University of California, Irvine
DOE	U.S. Department of Energy

Abbreviations & Acronyms	Name
V-I	Voltage Current